Alumina Hosts in Fe- and Al-rich Metapelites from Transangaria (Yenisey Ridge, East Siberia): Distribution, Composition, and Mining Potential

Ella V. Sokol , Svetlana N. Kokh , Anna V. Nekipelova , Igor I. Likhanov * , Anna S. Deviaitiarova , Pavel V. Khvorov

Posted Date: 3 August 2023

doi: 10.20944/preprints202308.0273.v1

Keywords: andalusite; kyanite; Fe- and Al-rich metapelites; Al2SiO5 concentrates; Yenisey Ridge

Article

Alumina Hosts in Fe- and Al-rich Metapelites from Transangaria (Yenisey Ridge, East Siberia): Distribution, Composition, and Mining Potential

Ella V. Sokol [1], Svetlana N. Kokh [1], Anna V. Nekipelova [1], Igor I. Likhanov [1,*], Anna S. Deviaitiarova [1] and Pavel V. Khvorov [2]

[1] V.S. Sobolev Institute of Geology and Mineralogy, Siberian Branch Russian Academy of Sciences, 3 Acad. Koptyug Avenue, 630090 Novosibirsk, Russia; sokol@igm.nsc.ru (E.V.S.); zateeva@igm.nsc.ru (S.N.K.); nekipelova@igm.nsc.ru (A.V.N.); likh@igm.nsc.ru (I.I.L.); devyatiyarova@igm.nsc.ru (A.S.D.)

[2] South Urals Federal Research Center of Mineralogy and Geoecology, Urals Branch, Russian Academy of Sciences, Institute of Mineralogy, Ilmeny Reserve Area, Miass 456317, Russia; khvorov@mineralogy.ru (P.V.K.)

* Correspondence: likh@igm.nsc.ru

Abstract: Fe- and Al-rich metapelite from the Transangarian segment of the Yenisey Ridge (East Siberia, Russia) is a potential new source of high-alumina refractories. The rocks have relatively high average contents of Al_2O_3 (20 wt.%) and Fe_2O_3 (7.91 wt%), moderate K_2O (3.44 wt%), and low CaO (0.74 wt%). Their dominant mineral assemblages are andalusite + muscovite + margarite + chlorite + biotite + quartz or staurolite + kyanite or/and andalusite + chlorite + muscovite + biotite + quartz with ±garnet and ±plagioclase. Al_2SiO_5 polymorphs occur as up to 1.5 cm andalusite porphyroblasts and partial or complete pseudomorphs after andalusite (kyanite and staurolite). Accessories include abundant Fe-Ti oxides and sporadic REE-, Y-, Ca-phosphates; sulfides are negligible. The composition of Al_2SiO_5 concentrates obtained in laboratory by heavy-media and magnetic separation from ≥0.06 mm fractions meet all requirements for raw material of this type: >56 wt% Al_2O_3, <42 wt% SiO_2, <1 wt% Fe_2O_3, <1.2 wt% TiO_2, and <0.2 wt% (CaO+MgO). The andalusite, kyanite, and mixed ores yield 0.7-4.1 wt%, 0.7-2.2 wt%, and 1.9-6.0 wt% of concentrate, respectively. The best-quality ores rich in Al_2SiO_5 polymorphs reside in zones of contact and/or dynamic metamorphism superimposed over regional metamorphism of Al-rich rocks.

Keywords: andalusite; kyanite; Fe- and Al-rich metapelites; Al_2SiO_5 concentrates; Yenisey Ridge

1. Introduction

Sillimanite-group minerals (SGM) comprising sillimanite (Sil), kyanite (Ky), and andalusite (And) are naturally occurring aluminosilicate polymorphs (Al_2SiO_5) remarkable by exceptional refractory properties. Being highly resistant to corrosion and high temperatures (up to 1500 °C), they are in high demand as raw material for the manufacturing of metals, glass, ceramics, and cement and have multiple uses in critical areas of furnaces, steel degassing chambers, foundry mold facings, etc. [1–7]. These minerals can be used as part of high-grade refractory composites or as a material for production of alloys (silumin or other Al alloys) and metallic alumina [1,8–10]. Currently, the production of high-grade Al_2SiO_5 concentrates is viable only from rich ores of a simple phase composition, which commonly occur in kyanite or sillimanite quartzites resulting from metasomatic alteration of polymineral metamorphic precursors, or less often in placers [2,3]. Economic andalusite is mainly found in contact-metamorphic pelitic schists in the thermal aureole of gabbroic or granitic plutons [3,11] and is mined from deposits that store at least 1×10^6 tons at SGM grades of ≥10-13 % for metamorphics and 1-2 % for placers [1–3,9,11].

Fe- and Al-rich metapelites with sillimanite-group rock-forming minerals, staurolite and chloritoid, and with high economic contents of Al_2O_3 ($X_{average} \approx 20$ wt%), occupy large areas in the Transangarian segment of the Yenisey Ridge due to a unique combination of protolith compositions

 doi:10.20944/preprints202308.0273.v1

and conditions of metamorphism [12–20]. The alumina-rich metamorphic rocks in the region may result from multi-stage And–Sil and Ky–Sil metamorphism of Fe- and Al-rich Early Proterozoic sediments [21]. By the time being, about forty sites of kyanite-sillimanite-andalusite mineralization have been discovered in the Transangarian Yenisey Ridge, mainly in the Lower Proterozoic Teya Group and the Middle Neoproterozoic Korda Fm. Numerous fields of Fe-Al-rich metamorphic rocks with 20-30 % of chloritoid ($(Fe^{2+},Mg,Mn^{2+})Al_2(SiO_4)O(OH)_2$) were also found within the Late Neoproterozoic Tungusik and Oslyanka Groups [15,18,22]. These areas posses large gold, manganese, lead, zinc, niobium, antimony, iron, and other mineral resources [23; 24] and thus have recently become a focus of growing interest as potential regional-scale sources of refractory raw materials and non-bauxite alumina.

Rocks with highest SGM percentages are mainly localized in Fe- and Al-rich metapelites of the Teya metamorphic complex in the central Yenisey Ridge. The rocks received much attention in the 1950s to 1980s in response to high alumina demand for the Russian industry which was satisfied for only 30 % from domestic sources. Exploration and mining performed in the 1979–1980 by the *Krasnoyarskgeologiya* survey in twenty areas within the central Yenisey Ridge revealed the Teya (Sil), Panimba (And), Mayakon, Chirimba (And-Ky), Kiya (And-Ky-Sil), and other potentially rich ore occurrences (Figure 1). In the 2000-2010s, the studies of metamorphic rocks in the region were mostly theoretical, e.g., in terms of the quantitative theory of metamorphism [16; 17; 25-27].

We provide the first detailed description of the mineralogy and chemistry of Fe- and Al-rich metapelites from the Mayakon and Panimba areas, as well as the compositions of their Al_2SiO_5 concentrates' and tailings, with production implications.

Preprints (www.preprints.org) | NOT PEER-REVIEWED | Posted: 3 August 2023 doi:10.20944/preprints202308.0273.v1

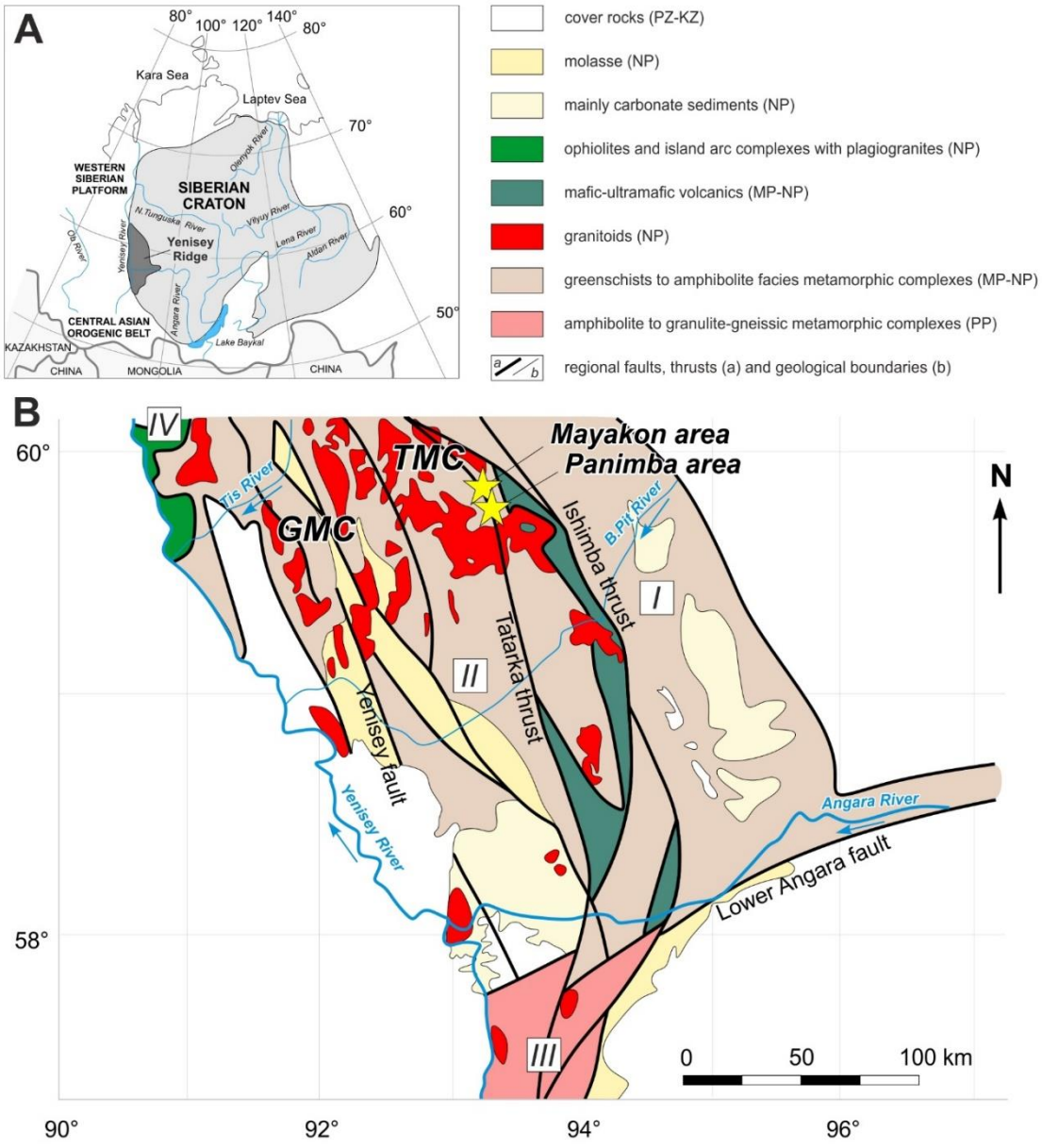

Figure 1. Location map of the Yenisey Ridge in the Siberian Craton (**A**, **inset**); Geological sketch map of the Yenisey Ridge (**B**) with locations of the Mayakon and Panimba areas (yellow stars) and tectonic blocks (Roman numerals in squares): East (craton) (I) and Central (II) blocks of the Transangarian segment, South-Yenisey (Angara-Kan) segment (III), and Isakovka island-arc block (IV). TMC = Teya metamorphic complex; GMC = Garevka metamorphic complex, modified after [21].

2. Geological Background

2.1. Regional Setting

The NW Yenisey Ridge striking 700 km along the Yenisey River in the western margin of the Siberian craton (Figure 1) is a Precambrian collisional-accretionary orogen, a part of the Central Asian Orogenic Belt [28]. The regional tectonic framework has traditionally been interpreted as a system of large-scale NW-SE isoclinal folds dipping to the NE, with regionally developed schistosity [29]. The Yenisey Ridge consists of the South Yenisey and North Yenisey (Transangarian) segments separated by the regional-scale W—E Lower Angara Fault (Figure 1). The Transangarian segment comprises the Meso-Neoproterozoic East and Central continental margin blocks and the Isakovka island arc terrane [30]. The tectonic blocks and terranes, from 300 to 500 km long and 50 to 80 km wide, are

 doi:10.20944/preprints202308.0273.v1

delineated by the Yenisey, Tatarka-Ishimba, and other large thrust faults often accompanied by smaller splay faults [17,26]. The deformation induced metamorphism of andalusite-sillimanite (low-pressure) and kyanite-sillimanite (medium-pressure) facies [13; 31, 32]. A detailed review of the geochronology, tectonic setting and geodynamic history of the region can be found in previous papers [15,28,33–35].

We sampled Fe- and Al-rich metapelites of the Teya metamorphic complex in the Panimba and Mayakon areas within the northern Transangarian segment of the Yenisey Ridge which consists of the Eastern and Central blocks separated by faults. The Central block accommodates the Garevka and Teya metamorphic complexes. The former includes the region's oldest rocks in its western part within the Yenisey shear zone and is overlain by the Lower Proterozoic Teya Group in the east. The Teya complex is located in the axial part of the Central block bounded by faults of the Tatarka-Ishimba suture zone (Figure 1). The Panimba and Mayakon areas are located in the east of the Central block, in the zone of the Tatarka-Ishimba regional fault.

The Teya complex is mainly composed of metacarbonate-clastic rocks of the Lower- and Middle-Proterozoic Teya and Sukhoy Pit Groups intruded by the Kalama calc-alkaline granites (*ca.* 850-860 Ma) with formation of a ~1 km wide zoned thermal aureole. The rocks show distinct metamorphic zonation from chloritoid to sillimanite-K-feldspar zones indicating a high temperature gradient ($dT/dZ \geq 100$ °C/km, where Z is the burial depth) [14,36].

The Panimba and Mayakon areas (Figures 2 and 3) are occupied by Middle Neoproterozoic metamorphic rocks of the Korda Fm. derived from a 1350-1250 Ma protolith. Low-pressure regional metamorphism at a gradient of $dT/dH = 25–35$ °C/km, common to orogenies, occurred between ~1050 Ma and ~950 Ma and produced Panimba- type And-Sil zoned complexes. Later the same rocks underwent moderate-pressure Ky–Sil collisional metamorphism (~850 Ma), with pressure locally elevated near thrusts of different sizes, at quite a low gradient of $dT/dH = 7–14$ °C/km. The resulting And-Ky metapelitic schists in the Mayakon and Panimba areas [17] contain up to 17 wt% And and/or up to 17 wt% Ky.

Preprints (www.preprints.org) | NOT PEER-REVIEWED | Posted: 3 August 2023 doi:10.20944/preprints202308.0273.v1

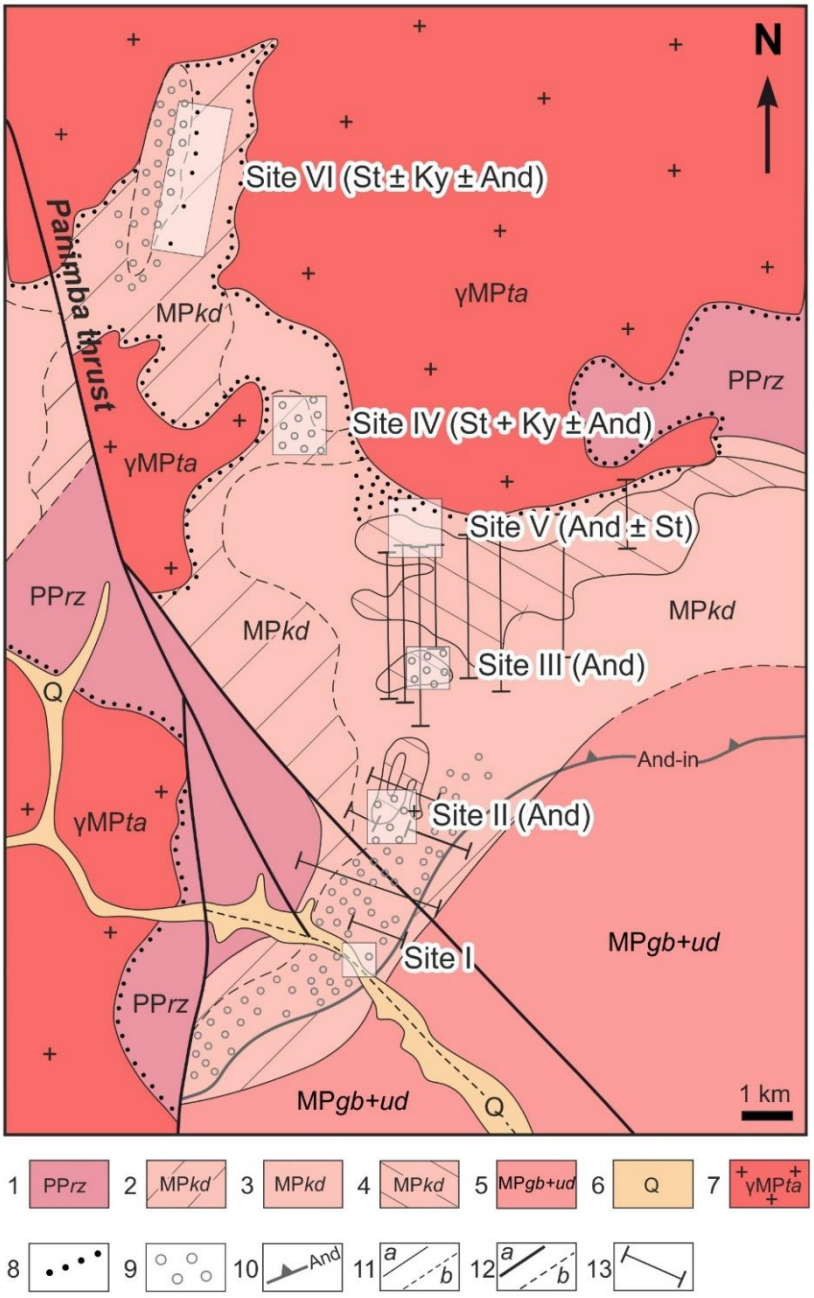

Figure 2. Simplified geology of the Panimba area, modified after [22]. 1 = Paleoproterozoic, Ryazanovka Formation (PP*rz*) of marble, calciphyre, and paramphibolite; 2-4 = Mesoproterozoic, Korda Formation (MP*kd*) of Ms-Bt (2) and And-bearing Grt-Ms-Bt (3) schists, 4 = And-enriched Grt-Ms-Bt-And schists (ore deposits); 5 = Mesoproterozoic, combined Goriblok and Uderei formations (MP*gb+ud*) of phyllite with interlayers of metamorphic siltstone; 6 = Cenozoic, Quaternary alluvium; 7 = Chirimba granitic pluton (γMP*ta*); 8 = Contact-metamorphic hornfels and marble; 9 = rocks affected by superimposed metamorphism; 10 = Andalusite isograde; 11 = observed (a) and inferred (b) geological boundaries; 12 = observed (a) and inferred (b) faults; 13 = Mines. Roman numerals I-VI are sampling sites. Abbreviations in braces are critical minerals.

Preprints (www.preprints.org) | NOT PEER-REVIEWED | Posted: 3 August 2023 doi:10.20944/preprints202308.0273.v1

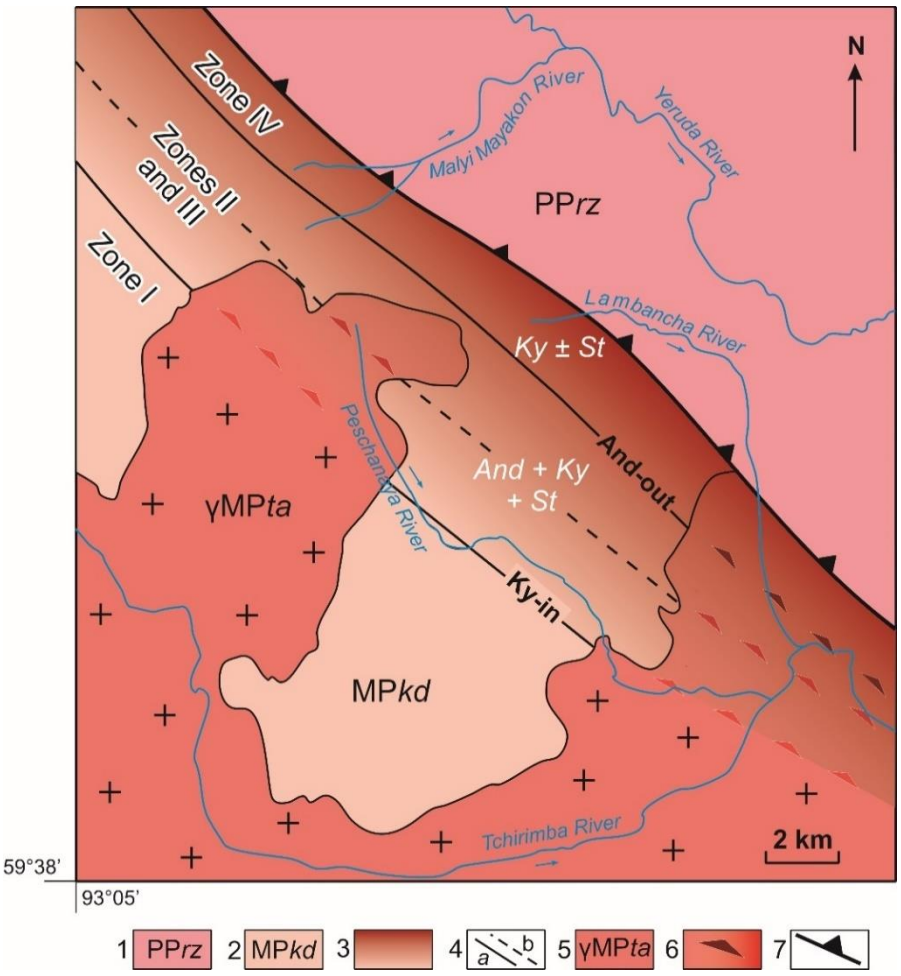

Figure 3. Simplified geology of the Mayakon area. 1 = Paleoproterozoic, Ryazanovka Formation (PP*rz*); 2-4 = Mesoproterozoic, Korda Formation (MP*kd*): 2 = metapelite of the Korda Formation produced by regional metamorphism (zone I); 3 = metapelite affected by collisional metamorphism (zones II-IV); 4 = And-Ky isograde (a) and boundaries between zones (b); 5 = Chirimba pluton (γMP*ta*); 6 = undifferentiated apogranitic cataclastic and blastoclastic rocks; 7 = Panimba thrust fault, modified after [17].

2.2. Sampling Areas and Metamorphic Conditions

The *Panimba area* is located in the southeastern part of the Teya metamorphic complex, in the middle reaches of the Panimba River within its divide with the Chirimba River (Figure 2). The metamorphic rocks of the area belong to the Korda Fm. and mainly consist of quartz-mica and quartz-chlorite-mica schists intercalated with lenses and layers of silty and quartzite sandstones. The rocks strike in the NW-SE direction and dip steeply (up to 60°). They are heavily deformed at hinges of large folds and are cut into blocks bounded by zones of shearing and mylonitization which host post-metamorphic gold mineralization [37].

Andalusite-bearing schists (mainly andalusite-quartz-mica varieties with andalusite-quartz-chlorite layers) are unevenly distributed among the Korda Fm. quartz-muscovite black shales following the originally heterogeneous lithology of the sedimentary protolith. The contents of andalusite range commonly from 3-5 to 10 wt% (7.8 wt% on average) in layers of meters to tens of meters thick but may reach 15-25 wt% in thin metapelite layers [22,37–39]. The rocks, with coarse banding and nodular structures due to randomly scattered andalusite porphyroblasts, provide one of the best illustrative examples of prograde *LP/HT* andalusite-sillimanite metamorphism in the Yenisey Ridge. Three regional metamorphic zones in metapelites were mapped in the SE to NW direction, toward increasing metamorphic grades (Figure 2) [22]: (1) Ms + Chl + Qz + Prl (sampling

Preprints (www.preprints.org) | NOT PEER-REVIEWED | Posted: 3 August 2023 doi:10.20944/preprints202308.0273.v1

site I); (2) Ms + Chl + Qz ± And ± Bt (sites II, III); (3) Ms + Chl + Qz + And + Bt ± Pl ± Grt ± St (site V). The prograde metamorphic zoning records shallow *LP/HT* andalusite-sillimanite regional metamorphism [40], from greenschist facies to the boundary of epidote-amphibolite facies [22]. Higher-pressure metamorphism occurred locally near the Panimba thrust (sites IV and VI, 1.5×0.6 km) and produced Ms + Chl + Qz + St + Bt ±And ± Ky ± Pl schists with up to 20 wt% kyanite, sporadic sillimanite, and rare remnant andalusite. Schists at sites II and III bear signatures of superimposed metamorphism, till the formation of white mica pseudomorphs after andalusite (Figure 4). The effect of the nearby Chirimba granite pluton shows up as sporadic cordierite (most often replaced) and scarce later sulfide mineralization (sites IV, V, and VI).

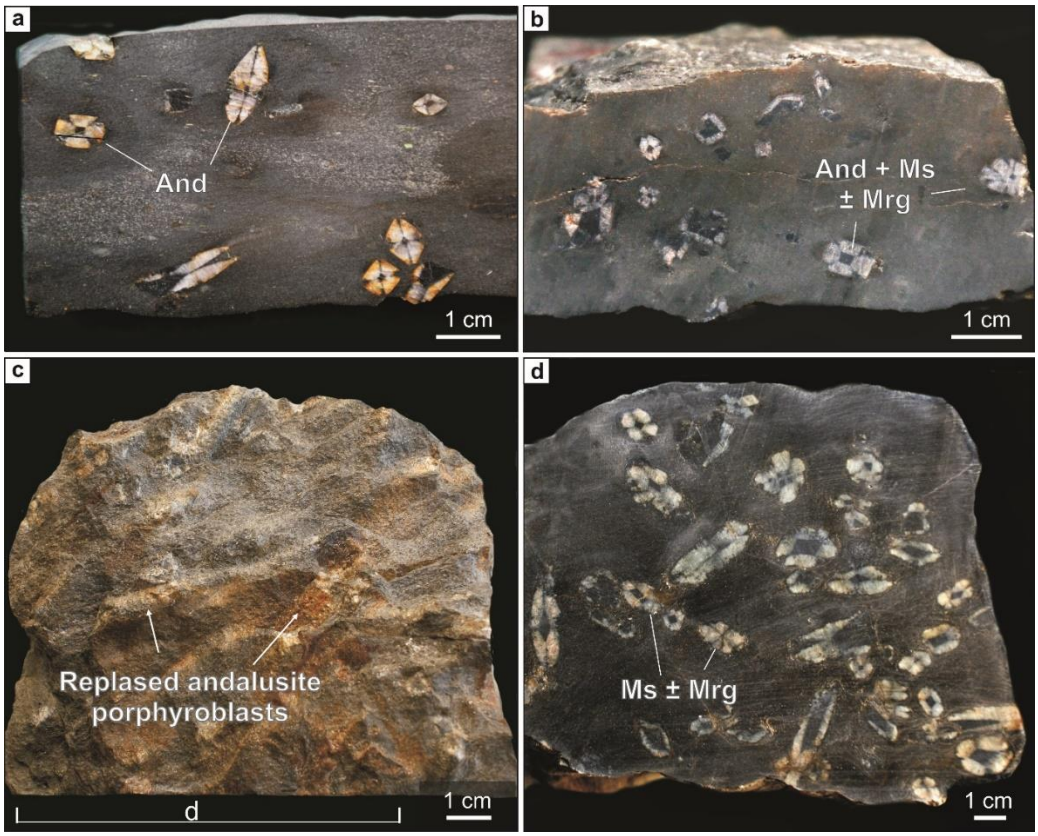

Figure 4. Low-pressure andalusite-bearing schists from Panimba area. Andalusite porphyroblasts partly or fully replaced by mica aggregates: (**a**) Fresh andalusite; (**b**) Partly replaced andalusite; (**c**, **d**) Andalusite fully replaced by white micas. Panels (c) and (d) show, respectively, naturally weathered and cut surfaces of samples. And = andalusite, Mrg = margarite, Ms = muscovite.

Andalusite-rich schists in the Panimba area (>10 km^2) are localized in two small sites, one in the south (650×40 m) and the other in the north (1200×(50-750) m) [39]. Both have irregular shapes and extend in the N—S direction, along the general strike of the metamorphic strata. Orebodies in the northern sites, contain at least 10 % andalusite (as evaluated from visual examination). The alumina resources stored in the Panimba andalusite-rich schists were estimated to reach 166 × 10^6 tons [22,39], assuming that the orebodies extend 200 m depthward and contain 10 wt% andalusite. The validity of the depth assumption was confirmed by exploratory drilling of the gold zone at the Panimba deposit, which showed the monoclinal bodies of andalusite schists and hornfels to reach depths more than 200 m, with bed thicknesses of 45-55 m near the surface and 10-35 m in deeper strata [37].

The *Mayakon area* lies north of the Panimba area, between the Yeruda and Chirimba Rivers, on the extension of the Korda Fm. carbonaceous andalusite schists (Figure 3). The Mayakon rocks underwent kyanite–sillimanite facies dynamic metamorphism superimposed on andalusite regional metamorphism of pelitic sediments. The area comprises two tectonic units separated by a thrust fault (Figure 3): the Korda plate southwest of the Panimba thrust lying under the Early Proterozoic

Preprints (www.preprints.org) | NOT PEER-REVIEWED | Posted: 3 August 2023 doi:10.20944/preprints202308.0273.v1

Penchenga plate in the northeast. The Korda Fm. metapelites were affected by later dynamic metamorphism in three zones up to 7 km wide parallel to the Panimba thrust. The Korda plate represents the Middle Neoproterozoic (~1000-865 Ma) regionally metamorphosed low-pressure andalusite-bearing metapelite overprinted by Neoproterozoic (~850 Ma) medium-pressure kyanite-bearing varieties [17]. The low-pressure mineral assemblages (And + Ms + Bt + Cld + Chl + Qz ± Pl ± Crd) were formed under the greenschist and epidote-amphibolite facies conditions (zone I, Figure 3); medium-pressure schists are composed of Ms + Bt + Chl + Qz + Grt + St + Ky ± Pl ± Cld with sporadic sillimanite and remnant andalusite [17]. According to geothermobarometry and *P-T* path calculations, pressure increase progressively from 3.5-4 kbar (zone I) to 4.5-5 kbar, 5.5-6 kbar (zones II and III, respectively) and finally to 6.2-6.7 kbar (zone IV) while mean maximum temperatures increase slightly from 560 to 580 °C towards the Panimba thrust. The minor temperature increase corresponds to a surprisingly low metamorphic gradient (dT/dZ) of about 5-7 °C/km during higher-pressure metamorphism. The maximum temperature (~600 °C) was inferred for sillimanite-bearing assemblages from intermediate zone III adjacent to granites and possibly affected by contact metamorphism recorded by cordierite-bearing assemblages in all zones [17]. The prograde evolution of mineral composition was supported by mass-transfer analysis of reactions showing gradual pressure rise during metamorphism at a nearly invariable temperature and bulk composition of the protolith. The relationships among Al_2SiO_5 polymorphs reveal successive replacement of andalusite by kyanite and occasionally by sillimanite (And→Ky→Sil) [40].

3. Materials and Methods

3.1. Sampling

The collections of Fe- and Al-rich metapelites with Al_2SiO_5 polymorphs comprised 20 and 26 samples from the Panimba and Mayakon areas, respectively. Both collections were sampled by Dr. Igor Likhanov and Dr. Pavel Kozlov during several field campaigns. Six representative samples from all rock groups (And-, And-Ky-, Ky-bearing schists, as well as samples subjected to later dynamic metamorphism of different grades), were selected for laboratory extraction of Al_2SiO_5 concentrates.

3.2. Ore Dressing

Laboratory experiments on extraction of Al_2SiO_5 concentrates from the high-alumina metapelites of the Teya metamorphic complex were performed at the V.S. Sobolev Institute of Geology and Mineralogy (Novosibirsk). The workflow consisted of several steps. First of all, the samples were crushed in a jaw crusher, milled, and screened into three size fractions (<0.06, 0.06≤x<0.1 and 0.1≤x<0.25 mm); the ≥0.06 mm fractions were used to obtain Al_2SiO_5 concentrates.

Step 1: magnetic separation. Magnetic (ferromagnetic and paramagnetic minerals) and non-magnetic components were separated on an induced roll magnetic separator (model 138T-SEM) (*Uralmekhanobr*, Sverdlovsk), at a magnetic intensity up to 1.0 T attainable in the gap between the feed pole and the roll. Samples were fed onto the roll and non-magnetic particles were thrown off the roll, whereas the magnetics were gripped, carried away from the field and deposited as magnetic product.

Step 2: heavy-medium separation. Non-magnetic products were placed into a separating funnel filled with $CHBr_3$ (density ≈ 2.89 g/cm^3), where minerals denser than the liquid were sinking and the lighter minerals were floating. The light and heavy products (concentrate lighter and heavier than 2.89 g/cm^3, respectively) were separated using a tap at the base of the funnel. The recovered material was washed with distilled water and dried.

Step 3: intense magnetic separation. Step 3 was performed on a UEM-1T magnetic analyzer (*GEOLOGORAZVEDK*A plant, Leningrad) designed for dry separation of low-magnetic materials. The instrument was set at 0.5 A current and 2.5 mm spacing of pole pieces, which ensured extraction of low-magnetic minerals as a separate product.

The three-step procedure eventually yielded a low-magnetic raw Al_2SiO_5 concentrate and a non-magnetic final Al_2SiO_5 concentrate (Figure 5).

Preprints (www.preprints.org) | NOT PEER-REVIEWED | Posted: 3 August 2023 doi:10.20944/preprints202308.0273.v1

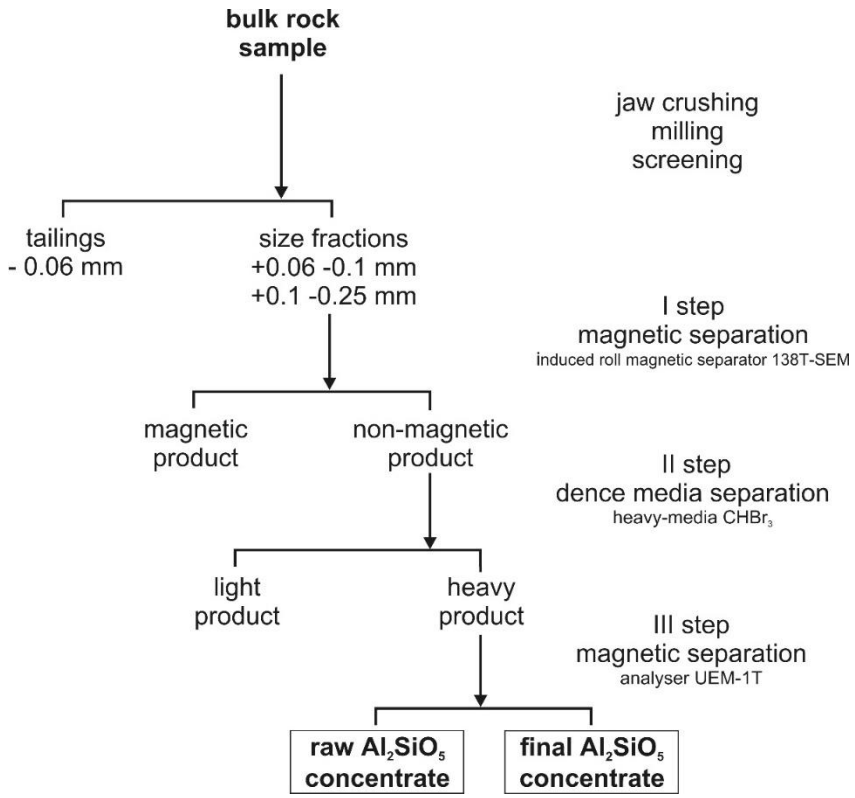

Figure 5. Flow chart for concentration procedure applied in this study.

3.3. Analytical Techniques

Analytical procedures were carried out at the Analytical Center for Multi-Elemental and Isotope Research (Sobolev Institute of Geology and Mineralogy, Novosibirsk, Russia), at the Geoanalitik shared research facilities (Zavaritsky Institute of Geology and Geochemistry (Yekaterinburg, Russia) and at the South Ural Research Center of Mineralogy and Geoecology (Miass, Russia).

Major elements in bulk rock samples, Al_2SiO_5 concentrates', and dressing products of andalusite and kyanite metapelites were analyzed by inductively coupled plasma atomic emission spectroscopy (ICP-AES) on a ThermoJarrell IRIS Advantage atomic emission spectrometer (Atkinson, WI, USA) at IGM (Novosibirsk). The preconditioning procedure included fusion of powdered whole-rock samples with lithium borate [42].

The contents of trace elements in bulk samples and Al_2SiO_5 concentrates from the andalusite and kyanite metapelites were determined by inductively coupled plasma mass spectrometry (ICP-MS) on a NexION 300S (PerkinElmer) quadrupole mass-spectrometer after microwave-assisted digestion using Speedwave MWS 3+ (Berghof) in the Geoanalitik shared research facilities of the IGG (Yekaterinburg). Preparation of analytical samples and analytical procedures followed the standard protocols as described in [43].

Metamorphic rock samples were prepared as polished thin sections and studied under transmitted polarized and reflected light using an Olympus BX51 optical microscope. Scanning electron microscopy (SEM) was applied to determine the texture and morphology of mineral grains and their aggregates. SEM was also applied to the products of all concentration steps. Mineral chemistry was analyzed by SEM from energy-dispersive spectra (EDS) and their distributions were visualized in elemental maps (EDS system) and back-scattered electron (BSE) images of carbon-coated samples (~15 to 25-nm carbon films). The measurements were performed on a Tescan Mira 3MLU scanning electron microscope (Tescan Orsay Holding, Brno, Czech Republic) equipped with an Oxford Aztec Energy Xmax-50 microanalyses system (Oxford Instruments Nanoanalysis, Abingdon, UK), at IGM (Novosibirsk). The operation conditions were: an accelerating voltage of 20

 doi:10.20944/preprints202308.0273.v1

kV and a beam current of 1 nA in low-vacuum (40-60 Pa) or high-vacuum modes, at a count time of 20 seconds.

Quantitative X-ray diffraction (XRD) analysis was applied to all examined samples of rocks and concentrates. Mineral phases (≥ 1 %) were identified by XRD in powdered samples. The measurements were performed on a Shimadzu XRD-600 diffractometer (Shimadzu Corporation, Kyoto, Japan) (CuKα radiation with a graphite monochromator, λ = 1.54178 Å), at SU FRC MG (Miass). The scans were recorded from 4–70 2θ at 0.02°2θ increments with 5 seconds scanning time per step. Quantitative mineralogical analysis on the basis of XRD was performed with the *Siroquant V4.1* software package (Sietronics, Mitchell, Australia; license number 11-10419406), using the *Siroquant* internal crystallographic database for minerals and inorganic materials.

Mineral abbreviations throughout the text are after [44].

4. Results

4.1. Chemistry, Mineralogy and Petrography of High Alumina Metapelites

4.1.1. Major- and Trace-Element Chemistry of Bulk Rock Samples

High-alumina schists from the Panimba and Mayakon areas have similar major- element compositions (Table 1). The rocks altered by regional (sites II, III and V; n = 10) and dynamic (sites IV and VI; n = 11) metamorphism in the *Panimba area* have, respectively, average contents of 19.81 and 21.06 wt% Al_2O_3, 8.49 wt% (6.38-10.33 wt%) and 8.70 wt% (6.16-10.92 wt%), Fe_2O_3. Few samples from sites IV and VI, with the lowest quartz percentages (7 to 35 wt%), bear considerable amounts of other Al hosts, besides Al_2SiO_5 polymorphs (15-36 wt%): micas (up to 48 wt%), staurolite (up to 15 wt%), and chlorite (up to 12 wt%), while bulk Al_2O_3 contents increase to 24-34 wt%. Other major oxides have similar respective concentrations in the regional and dynamic metamorphic rocks: 2.66-4.67 and 2.03-4.41 wt% K_2O; 1.30-3.01 and 1.33-3.62 wt% MgO; 0.85-1.17 and 0.72-1.74 wt% TiO_2; 0.12-1.45 and 0.08-1.58 wt% CaO; 0.16-2.09 and 0.12-2.18 wt% Na_2O; 0.03-0.20 and 0.03-0.26 wt% MnO.

Average Al_2O_3 contents in samples from the *Mayakon area* are 21.87 wt% (n = 2) in zone I, 19.97 wt% (n = 14) in zones II and III, and 19.92 wt% (n = 23) in zone IV (Table 1); Al_2O_3 is as high as 28.73 wt% in one sample from zone IV containing 16 wt% kyanite, 42 wt% micas (muscovite + biotite), 12 wt% chlorite and 6 wt% staurolite. The Mayakon samples have lower respective Fe_2O_3 and MgO contents than their counterparts from the Panimba area: 5.83-8.44 wt% and 1.85-1.94 wt% (7.13 and 1.89 wt% on average) in zone I; 6.15-8.76 wt% and 0.89-2.65 wt% (7.39 and 1.83 wt% on average) in zones II and III; 6.57-10.49 wt% and 1.16-2.62 wt% (8.49 and 1.93 wt% on average) in zone IV. The concentrations of Ti, K and Na oxides are moderate while P and Mn are low in all metamorphic zones of the area.

The Panimba and Mayakon metapelites were derived from the same Teya Group sedimentary protolith and thus share similar trace-element compositions (Table 2). The average concentrations of V (102 and 91.6 ppm) and Nb (13.3 and 10.3 ppm) are comparable with the upper continental crust (UCC) values [45], while Co (12.3 and 8.34 ppm), Ni (23.2 and 24.8 ppm), Cu (20.9 and 18.8 ppm), Zr (152 and 112 ppm), ΣREE (50.6 and 33.8 ppm), Th (4.53 and 3.43 ppm) and U (1.73 and 1.45 ppm) are slightly below the UCC concentrations. In general, the trace-element enrichment of the Teya metamorphic rocks is similar to that of high-Al rocks of the Keivy Group in the Kola Peninsula, Russia [46].

Preprints (www.preprints.org) | NOT PEER-REVIEWED | Posted: 3 August 2023 doi:10.20944/preprints202308.0273.v1

Table 1. Representative major element (in wt%) compositions of Fe- and Al-rich metapelitic schists from Panimba and Mayakon areas.

Sample	SiO_2	TiO_2	Al_2O_3	Fe_2O_3	MnO	MgO	CaO	Na_2O	K_2O	P_2O_5	BaO	LOI	Total
Panimba area, low-pressure schists (sites II, III and V)													
2	63.52	0.85	19.54	6.38	0.03	1.82	0.12	0.20	4.31	0.09	0.06	2.83	99.79
4	62.45	1.15	19.06	8.71	0.04	2.49	0.15	0.16	3.32	0.11	0.07	2.62	100.35
10*	61.56	1.04	18.77	9.49	0.06	3.01	0.19	0.16	4.00	0.08	0.07	1.89	100.37
11	61.62	0.99	19.74	7.06	0.06	1.53	0.15	0.32	4.20	0.05	0.08	4.24	100.05
11a	57.36	1.11	23.04	6.83	0.06	1.56	0.30	0.38	4.67	0.06	0.09	4.40	99.91
21	59.94	1.00	21.68	8.75	0.10	1.30	0.30	0.79	4.08	0.10	0.12	1.92	100.10
Minimum	57.06	0.85	18.18	6.38	0.03	1.30	0.12	0.16	2.66	0.05	0.06	0.99	—
Maximum	63.52	1.17	23.04	10.33	0.20	3.01	1.45	2.09	4.67	0.97	0.12	4.42	—
Average, n = 10	60.86	1.06	19.81	8.49	0.08	1.90	0.46	0.74	3.69	0.18	0.08	2.60	—
Panimba area, medium-pressure schists (sites IV and VI)													
14	59.67	0.97	20.32	8.20	0.08	2.37	0.16	0.35	3.60	0.07	0.07	4.26	100.19
22	41.47	1.74	33.75	10.92	0.26	1.85	0.70	1.87	4.33	0.08	0.14	2.50	99.62
27*	60.36	1.07	19.62	9.74	0.07	3.09	0.30	0.26	3.41	0.10	0.06	1.83	100.02
28*	63.29	0.91	20.01	6.92	0.06	2.23	0.17	0.25	4.10	0.07	0.07	1.87	100.03
30*	62.46	0.97	19.40	8.61	0.06	2.40	0.08	0.12	3.42	0.07	0.06	2.50	100.24
Minimum	41.47	0.72	13.12	6.16	0.03	1.33	0.08	0.12	2.03	0.04	0.05	1.29	—
Maximum	70.38	1.74	33.75	10.92	0.26	3.62	1.58	2.18	4.41	0.13	0.14	4.76	—
Average, n = 11	59.51	1.04	21.06	8.70	0.09	2.33	0.37	0.72	3.52	0.08	0.07	2.38	—
Mayakon area, zone I													
40	59.43	1.08	22.47	8.44	0.07	1.85	0.15	0.31	3.43	0.09	0.05	2.52	99.96
78	59.87	0.99	21.28	5.83	0.05	1.94	0.30	0.87	3.27	0.06	0.05	5.37	99.94
Average, n = 2	59.65	1.04	21.87	7.13	0.06	1.89	0.23	0.59	3.35	0.08	0.05	3.95	—
Mayakon area, zones II and III													
36a*	60.41	0.96	23.29	7.60	0.04	1.37	0.28	1.01	3.45	0.11	0.07	1.44	100.09
44	60.77	1.15	24.41	6.80	0.05	1.22	0.18	0.23	3.21	0.11	0.04	1.33	99.52
51	58.25	1.20	22.47	6.70	0.14	0.89	0.68	1.32	3.82	0.52	0.08	3.46	99.60
62	67.86	0.97	15.02	7.04	0.06	1.64	0.17	0.29	3.13	0.07	0.07	3.25	99.58
64	62.07	0.94	19.25	7.35	0.05	1.83	0.23	0.43	3.89	0.09	0.08	3.68	99.94
66	66.78	1.04	16.44	7.40	0.07	2.03	0.32	0.30	3.13	0.11	0.07	1.63	99.33
Minimum	58.02	0.73	13.87	6.15	0.04	0.89	0.16	0.13	1.96	0.07	0.03	1.33	—
Maximum	73.51	1.20	24.41	8.76	0.14	2.65	0.68	1.32	3.89	0.52	0.08	4.81	—
Average, n = 14	62.80	0.97	19.97	7.39	0.07	1.83	0.29	0.45	3.20	0.12	0.06	2.44	—
Mayakon area, zone IV													
38	62.82	0.97	18.37	8.37	0.06	1.95	0.09	0.11	2.94	0.08	0.04	3.65	99.54
39	59.06	1.02	21.25	7.96	0.07	1.90	0.23	0.54	4.44	0.08	0.07	3.59	100.22
50	61.44	1.21	19.07	8.69	0.11	1.41	0.46	0.74	3.73	0.25	0.10	2.90	100.16
57	48.83	1.09	28.73	7.56	0.04	1.85	1.08	0.67	4.51	0.11	0.08	4.43	99.00
70*	56.82	0.99	22.99	8.35	0.07	2.25	0.16	0.43	3.52	0.08	0.07	3.54	99.34
73	60.29	0.96	19.38	8.79	0.11	2.57	0.45	0.44	3.61	0.06	0.07	3.31	100.12
Minimum	48.83	0.55	11.24	6.34	0.04	1.16	0.09	0.11	2.12	0.05	0.02	2.33	—
Maximum	69.02	1.30	28.73	10.49	0.23	2.62	1.43	1.11	4.51	0.45	0.11	4.43	—
Average, n = 23	60.37	0.98	19.92	8.49	0.09	1.93	0.39	0.53	3.57	0.12	0.07	3.32	—

* = samples from which Al_2SiO_5 concentrates were extracted. All iron is calculated as Fe_2O_3. LOI = loss on ignition.

Preprints (www.preprints.org) | NOT PEER-REVIEWED | Posted: 3 August 2023 doi:10.20944/preprints202308.0273.v1

Table 2. Representative trace-element (in ppm) compositions of Fe- and Al-rich f metapelitic schists from Panimba and Mayakon areas.

Sample	V	Cr	Co	Ni	Cu	Zr	Nb	Th	U	∑REE
Panimba area, low-pressure schists (areas II, III and V)										
2	80	60	6	17	24	240	21	3.3	3.3	22.6
4	100	130	15	36	15.6	300	20	4.5	2.3	40.0
10*	120	90	17	32	34	140	12	4.6	2.1	50.3
11	130	80	6	20	15.8	160	13	4.2	2.3	27.1
11a	160	90	5	19	24	140	13	4.9	1.7	32.5
21	90	100	15	25	26	120	12	2.7	1.5	20.4
Minimum	70.0	60.0	5.00	15.0	11.7	120	12.0	2.0	1.40	20.4
Maximum	160	130	24.0	36.0	36.0	300	21.0	4.9	3.30	50.3
Average, n = 10	100	84.0	12.3	25.6	23.8	178	15.0	3.69	1.99	36.2
Panimba area, medium-pressure schists (areas IV and VI)										
14	140	130	10	25	22	120	12	2.9	1.7	20.6
22	110	90	18	23	13	240	26	4.4	2.6	45.8
27*	130	130	21	40	33	110	11	2.9	1.2	16.4
28*	130	80	9	16	12.3	110	11	2.9	1.6	22.1
30*	130	80	8	17	17.8	130	11	9	1.9	109
Minimum	40.0	40.0	2.60	9.00	11.8	82.0	8.00	1.40	0.80	11.9
Maximum	140	150	21.0	40.0	33.0	240	26.0	13.9	2.60	205
Average, n = 11	105	94.5	11.2	21.1	18.3	129	11.8	5.3	1.50	63.7
Mayakon area, Zone I										
40	100	90	9.0	33	23	110	12	9	1.8	87.5
78	100	130	5.0	22.0	9.0	130	14.0	1.9	1.3	10.5
Average, n = 2	100	110	7.0	27.5	16.0	120	13.0	5.5	1.6	49.0
Mayakon area. Zones II and III										
36a*	100	80	10	17	12.6	110	10	5	1.5	65.4
44	140	100	12	20	17	120	13	1	3.1	2.29
62	90	60	7	36	17.8	110	10	4.7	1.4	46.3
64	90	60	7	36	17.8	82	8	2.4	1.3	238
66	70	50	5	15	6	66	6.2	2.7	0.9	19.4
Minimum	30.0	40.0	4.00	7.00	6.00	66.0	5.00	0.21	0.80	0.73
Maximum	140	110	12.0	37.0	25.0	160	16.0	6.0	3.10	65.4
Average, n = 14	92.0	70.0	7.7	20.4	14.4	110	10.2	2.57	1.44	22.6
Mayakon area. Zone IV										
38	110	80	6	29	23	110	10	8	1.4	130
39	100	90	8	24	10	99	11	10	1.7	114
50	80	60	9	23	16.3	160	13	1.8	1.6	13.7
57	120	90	10	25	11.1	150	12	2.6	2	23.2
70*	130	330	11	80	10	120	13	3.1	2.4	11.6
73	120	100	11	36	8	120	12	4.4	2.1	28.3
Minimum	40.0	34.0	2.80	9.00	8.00	57.0	3.20	1.10	0.90	4.67
Maximum	130	330	16.0	80.0	110	170	17.0	10.0	2.4	130
Average, n = 23	95.0	90.2	9.4	29.1	23.3	117.4	10.5	4.1	1.5	42.4

* = samples from which Al_2SiO_5 concentrates were extracted.

Preprints (www.preprints.org) | NOT PEER-REVIEWED | Posted: 3 August 2023 doi:10.20944/preprints202308.0273.v1

4.1.2. Petrography

The analyzed samples of regional metamorphic rocks from the *Panimba area* mostly contain more than 40 wt% quartz (44.5 wt% on average). Micas show especially high percentages (27-46 wt%, average 36.2 wt%) in rocks affected by superimposed metamorphism (sites II and III) and are the lowest in dynamic metamorphic rocks (11-24 wt%; average 19.9 wt%, n = 8 in site VI). Fe-rich chlorite is present in most of the rocks (1-2 to 20 wt%, 7.6 wt% on average, n = 12) but mainly lacks in rocks from the site of dynamic metamorphism (site VI) where it reaches 5 wt% in a single sample. Instead, high-Al assemblages in this site (Figure 6), as well as in sites IV and V, include staurolite (5-20 wt%; 7.8 wt% on average, n = 12), which often becomes main Al host rather than Al_2SiO_5 polymorphs.

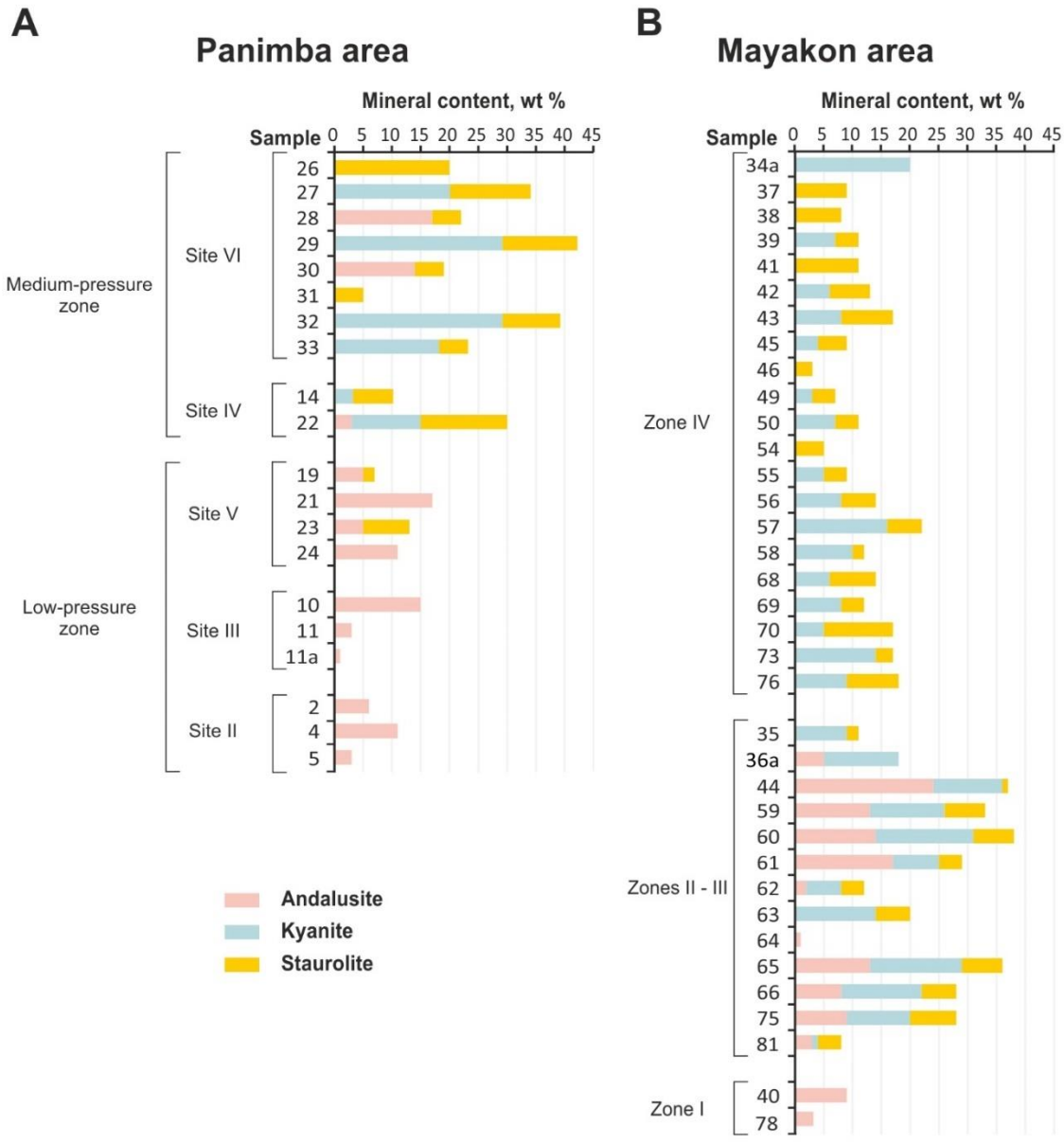

Figure 6. Percentages (wt %) of andalusite, kyanite, and staurolite in Fe- and Al-rich metapelites from Panimba (**A**) and Mayakon (**B**) areas, according to XRD data.

The Panimba andalusite (up to 15 wt%) porphyroblastic schists are medium- to coarse-grained with a matrix composed of quartz, chlorite, muscovite, and biotite with accessory ilmenite, rutile, monazite and very rare zircon, fluorapatite, xenotime, tourmaline, thorianite and zincite (Table 3 and Figures 6, 7 and 8a,b). Quartz, the most abundant phase, occurs as irregular grains up to 0.5 mm in diameter with straight and oval-shaped margins. Flakes of biotite, muscovite and chlorite, up to 500

Preprints (www.preprints.org) | NOT PEER-REVIEWED | Posted: 3 August 2023 doi:10.20944/preprints202308.0273.v1

μm in length, are abundant as well. Ilmenite, rutile and phosphates are commonly dispersed in the quartz-biotite-chlorite matrix. In some samples, clusters of quartz grains are accompanied by monazite and xenotime aggregates (Figure 8a). Andalusite porphyroblasts (often chiastolitic), up to 1.5 cm in diameter, are often replaced by margarite and muscovite. Margarite veinlets of early replacement stages cut the andalusite porphyroblasts, while margarite laths grow perpendicular to the walls. Andalusite grains are rimmed with fan-like muscovite aggregates (Figures 7a-c and 9). Both margarite veinlets and muscovite rims enclose accessory minerals (Figure 9). The Panimba schists contain widespread muscovite pseudomorphs after chiastolite which preserve the chiastolite shapes and inclusion patterns (Figure 7d).

Table 3. Diversity of accessories in metapelites from Panimba and Mayakon areas (SEM data).

Mineral	Formula	Mayakon Area			Panimba Area	
		Zone I	Zones II-III	Zone IV	Sites II-III	Sites IV-VI
Oxides and Silicates						
Ilmenite	$FeTiO_3$	●●	●●●	●●	●●●	●●●
Rutile	TiO_2			●●	●●	○
Zircon	$Zr(SiO_4)$	●	●	●	●	●
Zincite	ZnO				○	○
Thorianite	ThO_2				○	○
Phosphates						
Monazite-Ce	$LREE(PO_4)$	●●	●●	●●	●●	●●
Xenotime-Y	$(Y,HREE)(PO_4)$			○	●	●
Fluorapatite	$Ca_5(PO_4)_3F$		●	○	○	
Sulfides						
Pyrite	$FeS_{2\ cub}$					●●
Pyrrhotite	$Fe_{1-x}S$		○	○	○	●
Chalcopyrite	$CuFeS_2$					○
Cubanite	$CuFe_2S_3$					○
Galena	PbS					○
Molybdenite	MoS_2					○
Bi-Te sulfide						○
Ag sulpfide				○		
Sulfates						
Barite	$BaSO_4$					○

Symbols show relative mineral content: ●●● = main phase; ●● = abundant phase; ● = rare phase; ○ = sporadic phase; no symbol = absent.

Schists near the Panimba thrust (sites IV and VI) often contain porphyroblastic andalusite (up to 17 wt%) crystals, partially to fully replaced by kyanite-staurolite-quartz-muscovite pseudomorphs (Figures 6 and 7e,f) but preserving remnant andalusite in the cores and the outline of original andalusite crystals. Kyanite (up to 29 wt%) is coarse grained (up to 1 mm) and occurs as randomly oriented blades and radial sheaves. Idioblastic ≤0.7 mm pale-yellowish crystals of staurolite (up to 20 wt%) have vermicular quartz intergrowths localized at the cores. Quartz (up to 300 μm) is the predominant matrix mineral. Lepidoblastic grains (≤700 μm) of brownish biotite exhibit kink bands in the matrix and along the grain boundaries of pseudomorphs after andalusite. Chlorite and muscovite occur in the matrix as fine flakes, while plagioclase forms irregular grains. Accessories include abundant ilmenite and monazite, rare zircon and xenotime, as well as single grains of rutile, zincite, thorianite and barite (Table 3).

Preprints (www.preprints.org) | NOT PEER-REVIEWED | Posted: 3 August 2023 doi:10.20944/preprints202308.0273.v1

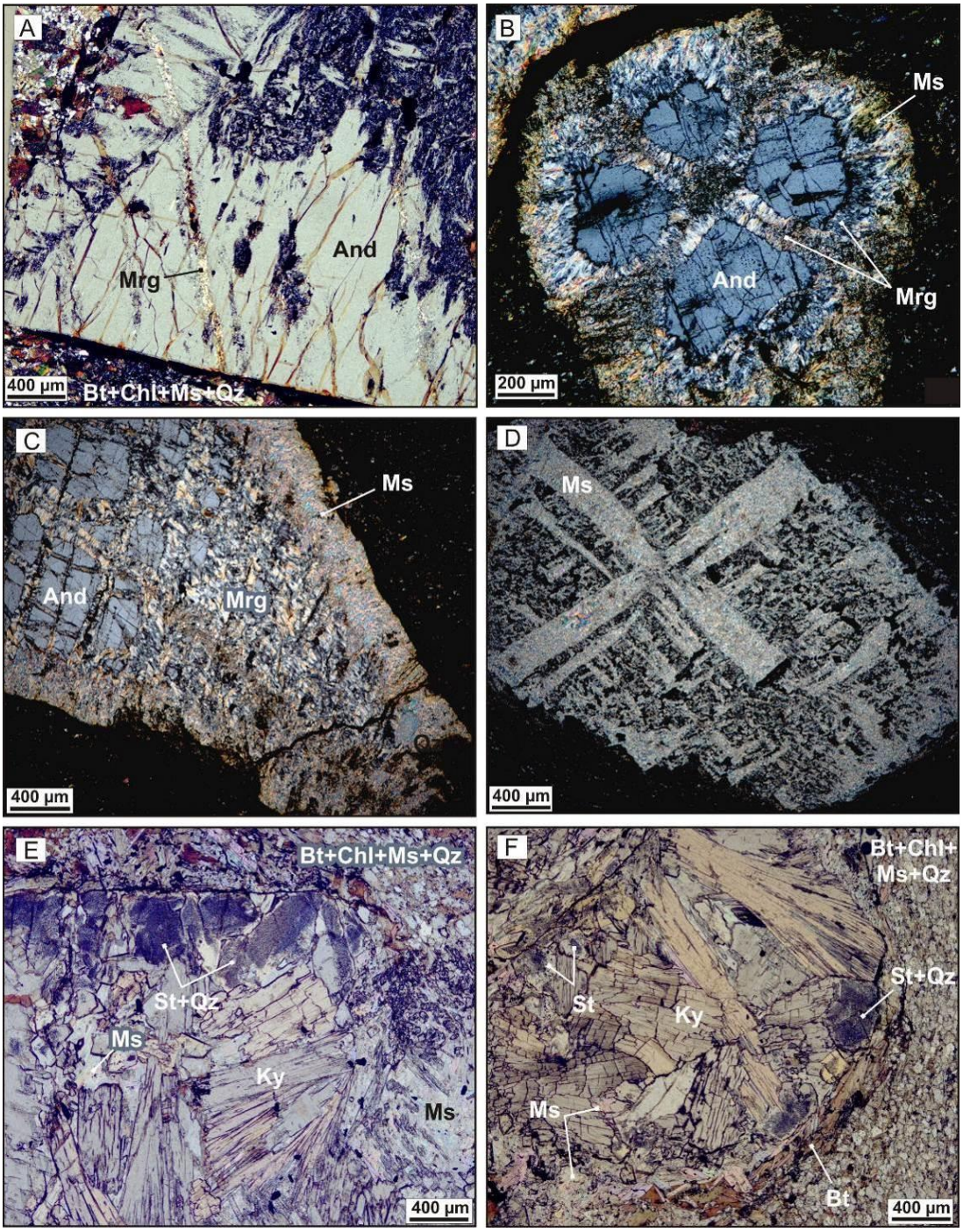

Figure 7. Photomicrographs of the Panimba Fe- and Al-rich metapelites, cross-polarized light (A–D) and plane-polarized light (E,F): (**A-D**) Low-pressure andalusite-bearing schists. Andalusite porphyroblasts partly to fully replaced by margarite and muscovite aggregates, from almost fresh andalusite with sporadic margarite veinlets (A), to partly replaced andalusite with margarite veinlets and muscovite rims (B,C), till complete muscovite pseudomorphs after chiastolitic andalusite (D); (**E, F**) Medium-pressure kyanite-bearing schists. Porphyroblastic andalusite crystals fully replaced by kyanite-staurolite-quartz-muscovite pseudomorphs. And = andalusite, Bt = biotite, Chl = chlorite, Ky = kyanite, Mrg = margarite, Ms = muscovite, Qz = quartz, St = staurolite.

Preprints (www.preprints.org) | NOT PEER-REVIEWED | Posted: 3 August 2023 doi:10.20944/preprints202308.0273.v1

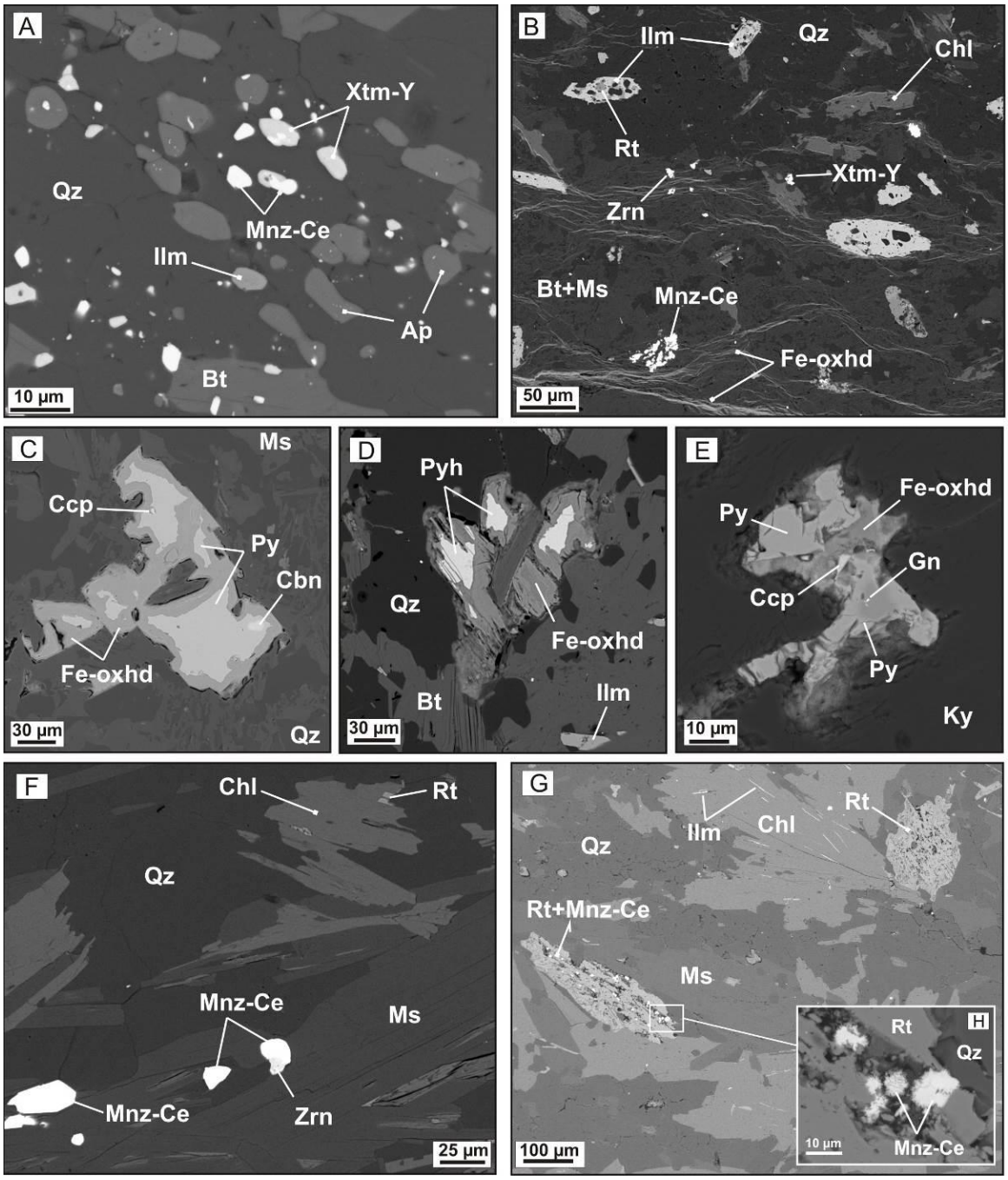

Figure 8. Back-scattered electron (BSE) images of accessory minerals in the Panimba (A-E) and Mayakon (F-H) metapelites: (**A**) Fine-grained phosphates (monazite, xenotime, and fluorapatite) in an aggregate of quartz grains; (**B**) Phosphates (monazite, xenotime, and fluorapatite), zircon and Fe-Ti oxides (ilmenite and rutile) scattered in quartz-biotite-chlorite-muscovite matrix; (**C, D**) Sulfide mineralization in mica-rich matrix of metapelites from contact with granitic rocks in the Panimba area. Sulfides are partly replaced by Fe^{3+}-(oxi)hydroxides; (**E**) Inclusion of intergrown pyrite, chalcopyrite, and galena in kyanite within a pseudomorph after andalusite, from contact with granitic rocks, Panimba area; (**F-H**) Distribution of monazite, zircon, ilmenite, and rutile in mica-rich matrix. Ap = fluorapatite, Bt = biotite, Cbn = cubanite, Ccp = chalcopyrite, Chl = chlorite, Fe-oxhd = Fe^{3+}-(oxi)hydroxides, Gn = galena, Ilm = ilmenite, Ky = kyanite, Mnz-Ce = monazite, Ms = muscovite, Py = pyrite, Pyh = pyrrhotite, Qz = quartz, Rt = rutile, Xtm-Y = xenotime, Zrn = zircon.

Preprints (www.preprints.org) | NOT PEER-REVIEWED | Posted: 3 August 2023 doi:10.20944/preprints202308.0273.v1

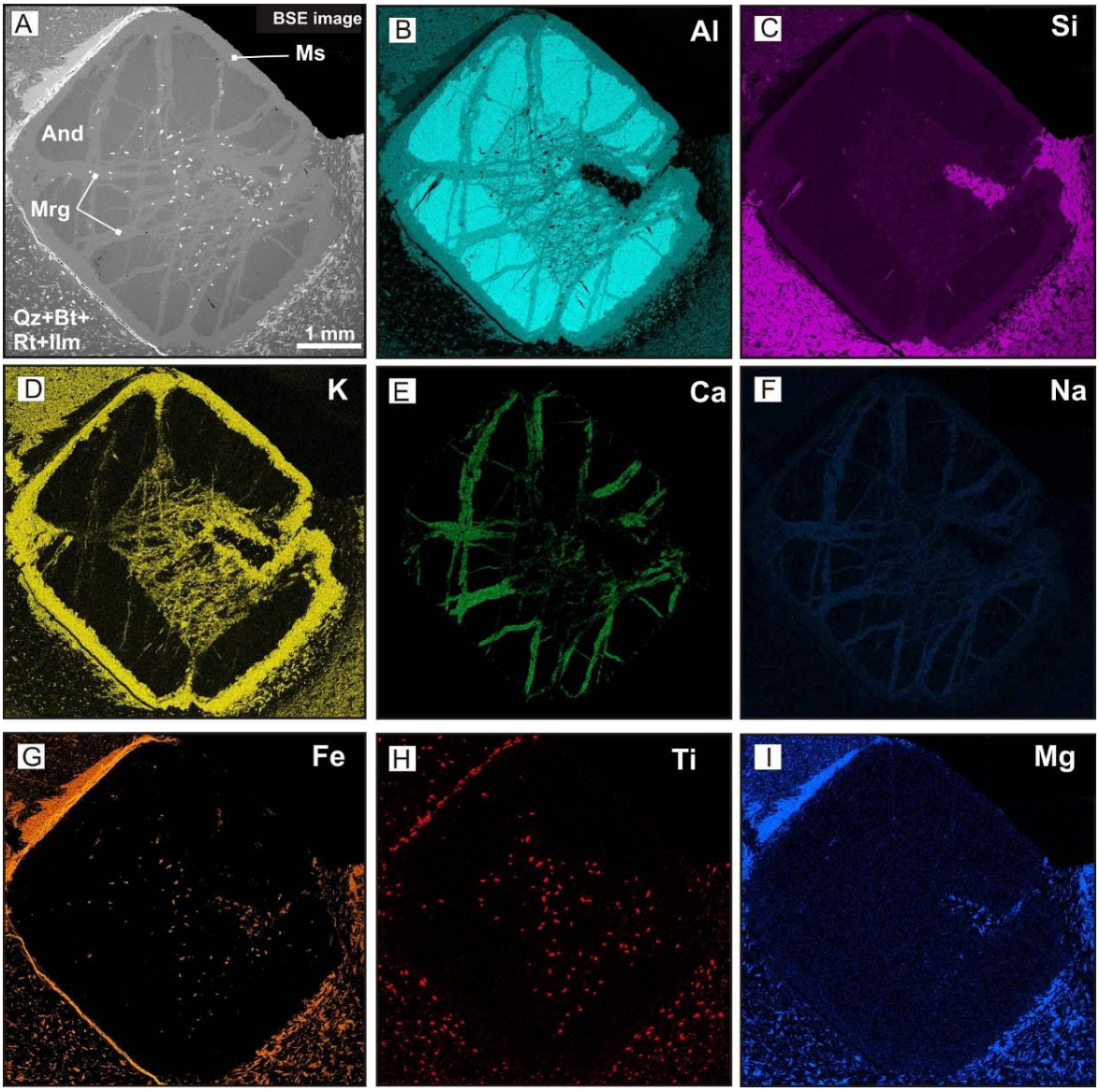

Figure 9. Back-scattered electron (BSE) image (**A**) and elemental maps (Al, Si, K, Ca, Na, Fe, Ti, Mg) (**B-I**) of andalusite porphyroblast from Panimba metapelites. Ca distribution within the andalusite porphyroblast reflects margarite veinlets; K distribution around the porphyroblast highlights a muscovite rim. Fe and Ti elemental maps show distribution of rutile and ilmenite inclusions localized in chiastolitic core, margarite veinlets, and quartz-chlorite-biotite matrix. And = andalusite, Bt = biotite, Ilm = ilmenite, Mrg = margarite, Ms = muscovite, Qz = quartz, Rt = rutile.

Sulfides are low to absent in the schists that are rich in andalusite and/or kyanite but are abundant and diverse (pyrite, pyrrhotite, chalcopyrite and, less often, sphalerite, arsenopyrite, marcasite, and galena) in the schists, hornfels, and blastomylonite rocks from the gold zones of the Panimba area [37]. Scarce but quite diverse sulfide mineralization, with predominant pyrite, pyrrhotite, and chalcopyrite, rare cubanite, molibdenite, galena, and single grains of Bi and Te sulfides, was found only in schists from sites IV-VI (near the Chirimba pluton) where sulfide minerals coexist with accessory phosphates and Fe-Ti oxides. Fe- and Fe-Cu sulfides are often oxidized and replaced by Fe^{3+}-(oxy)hydroxide aggregates (Table 3 and Figure 8c-e).

The metapelite samples from the Mayakon area have variable percentages of quartz, from 20 to 63 wt%, higher in samples from zones II and III (47.9 wt% on average, n = 13), lower in rocks from zone I (44.0 wt% on average n = 2), and lowest in zone IV (42.3 wt% on average, n = 21). Chlorite is present in most of samples from zones I and IV and in one third of those from zones II-III (6-19 wt%, 10.9 wt % on average, n = 23). Micas reach the highest percentages in rocks from zone I (35-38 wt%,

Preprints (www.preprints.org) | NOT PEER-REVIEWED | Posted: 3 August 2023 doi:10.20944/preprints202308.0273.v1

36.5 wt% on average, n = 2), are slightly lower in zone IV samples (21-49 wt%, 32.2 wt% on average, n = 21), and the lowest in those from zones II and III (8-43 wt%, average – 23.3 wt%; n = 13).

Typical metapelites of zone I consist of andalusite (up to 9 wt%), muscovite, quartz, biotite, and chlorite (Figure 6), with accessory ilmenite, rutile, monazite, and zircon (Table 3). They contain chiastolitic andalusite crystals, up to 1 cm in diameter, but lack kyanite and staurolite. Andalusite is fresh or locally replaced by muscovite (Figure 10a,b). Quartz occurs as irregular grains, up to 0.5 mm in diameter. Biotite, muscovite, and chlorite flakes (up to 1 mm in length) define foliation in the rocks.

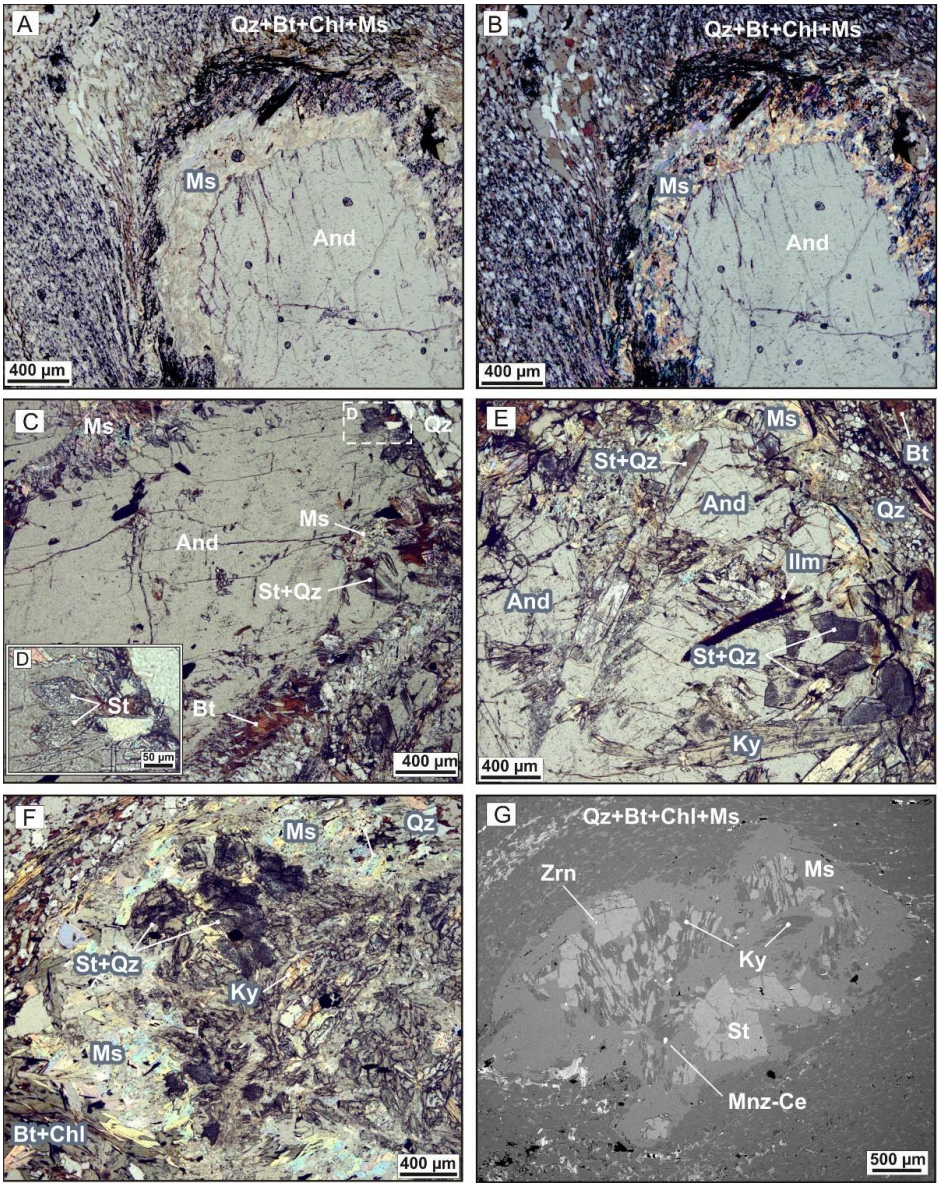

Figure 10. Photomicrographs and a back-scattered electron image (G), plane-polarized light (A, C, D-F) and cross-polarized light (B). of the Mayakon metapelites: (**A,B**) Andalusite porphyroblast with muscovite rim from zone I; (**C-E**) Andalusite crystals replaced by kyanite, staurolite, muscovite, and quartz aggregates along fractures and margin of grains (C,E); vermicular quartz intergrowth texture in staurolite from zones II-III (D); (**F,G**) Complete kyanite-staurolite-muscovite-quartz pseudomorphs after andalusite porphyroblasts from zone IV. And = andalusite, Bt = biotite, Chl = chlorite, Ilm = ilmenite, Ky = kyanite, Mnz-Ce = monazite, Mrg = margarite, Ms = muscovite, Qz = quartz, St = staurolite, Zrn = zircon.

The mineral assemblage in metapelitic rocks from zone IV includes kyanite (up to 16 wt%), staurolite (up to 11 wt%), biotite, chlorite, muscovite, garnet, plagioclase and quartz with accessory

Preprints (www.preprints.org) | NOT PEER-REVIEWED | Posted: 3 August 2023 doi:10.20944/preprints202308.0273.v1

ilmenite, rutile, monazite, zircon, and very rare xenotime and fluorapatite (Table 3 and Figure 6). Andalusite porphyroblasts (up to 1 cm) are fully converted into kyanite-staurolite-muscovite-quartz aggregates (Figure 10f,g), and no remnant andalusite is preserved in pseudomorphs. Garnet exists as large (up to 1.5 cm) porphyroblasts with staurolite, quartz and ilmenite inclusions. Some garnets show spiral-shaped inclusion fabrics (snowball structures) reflecting syntectonic growth of rotating porphyroblasts.

4.1.3. Chemistry of Minerals

Mineral chemistry is illustrated by representative analyses summarized in Tables 4–12.

Andalusite and *kyanite* in all samples are close to the ideal stoichiometry with 0.24-0.41 wt% and 0.27-0.63 wt% Fe_2O_3, respectively (Table 4).

Staurolite in all analyzed samples shows consistent Fe-rich composition (X_{Fe} = 0.83-0.88) with 0.50-0.60 wt% TiO_2 and 0.21-0.44 wt% MnO. Staurolite in the Mayakon samples also contain 0.45-0.92 wt% ZnO (Table 5).

Garnets mostly have almandine compositions (76.7-82.8 mol%), with lesser percentages of pyrope (8.0-11.1 mol%), grossular (4.9-9.5 mol%), and spessartite (0.8-5.7 mol%) (Table 5). TiO_2 and Cr_2O_3 are always below their detection limits. Garnet crystals are generally unzoned.

Plagioclase is generally albite-rich (Ab_{81-86}) with minor (less than 1.6 %) orthoclase, while that in metapelites of zone IV (Mayakon area) is more anorthite-rich (Ab_{62-66}).

Table 4. Representative compositions of andalusite and kyanite from metapelites of the Panimba and Mayakon areas. SEM EDS data (in wt%).

Mineral	**Andalusite**								**Kyanite**				
Area	P	P	P	P	P	M	M	M	P	P	M	M	M
Sample	2	4	11a-1	21	21	60	60	60	29	29	45	5	85
SiO_2	36.52	36.71	35.88	35.98	35.96	36.11	36.05	36.05	36.3	35.98	36.73	36.56	37.20
Al_2O_3	63.39	63.47	62.90	63.43	63.24	63.66	63.01	63.11	62.88	62.60	63.22	62.24	62.98
Fe_2O_3	0.26	0.24	0.31	0.41	0.30	0.31	0.29	0.39	0.31	0.51	0.27	0.63	0.29
Total	100.17	100.42	99.09	99.82	99.50	100.08	99.35	99.55	99.49	99.09	100.22	99.43	100.47
Formula based on 5 oxygens, apfu													
Si	0.985	0.987	0.979	0.975	0.977	0.975	0.981	0.979	0.986	0.982	0.990	0.994	1.000
Al	2.015	2.012	2.022	2.025	2.025	2.027	2.020	2.020	2.013	2.014	2.008	1.995	1.995
Fe^{3+}	0.005	0.005	0.006	0.008	0.006	0.006	0.006	0.008	0.006	0.010	0.005	0.013	0.006
Total	3.005	3.004	3.007	3.008	3.008	3.008	3.006	3.007	3.005	3.006	3.003	3.002	3.000

apfu = atoms per formula unit; P = Panimba area, M = Mayakon area. TiO_2, MnO, MgO, CaO, Na_2O, and K_2O are below detection limit (<0.20 wt%).

Table 5. Representative compositions of staurolite and garnet from metapelites of the Panimba and Mayakon areas. SEM EDS data (in wt%).

Mineral	**Staurolite**							**Garnet**	
Area	P	P	P	M	M	M	M	M	M
Sample	27	29	29	45	57	57	60	39	39
SiO_2	27.47	26.81	27.70	27.41	26.83	26.64	26.70	36.71	36.86
TiO_2	0.55	0.50	0.60	<0.20	<0.20	<0.20	0.55	<0.20	<0.20
Al_2O_3	52.92	53.30	53.08	54.49	53.62	54.66	53.34	20.95	20.67
FeO	14.04	13.78	13.42	13.25	13.46	13.50	14.67	37.24	35.06
MnO	0.22	0.44	0.43	<0.20	0.21	<0.20	0.25	0.36	2.58
MgO	1.26	1.59	1.41	1.04	1.06	1.03	1.08	2.79	2.06
ZnO	<0.20	<0.20	<0.20	0.45	0.65	0.92	<0.20	<0.20	<0.20
CaO	<0.20	<0.20	<0.20	<0.20	<0.20	<0.20	<0.20	2.04	3.39
Total	96.46	96.42	96.64	96.64	95.83	96.75	96.59	100.09	100.62

Preprints (www.preprints.org) | NOT PEER-REVIEWED | Posted: 3 August 2023 doi:10.20944/preprints202308.0273.v1

Formula based on	46 oxygens, apfu							24 oxygens, apfu	
Si	7.746	7.573	7.778	7.683	7.621	7.499	7.553	5.943	5.959
Ti	0.117	0.106	0.127	0.000	0.000	0.000	0.117	0.000	0.000
Al	17.587	17.742	17.565	18.000	17.950	18.134	17.783	3.997	3.938
Fe^{2+}	3.311	3.255	3.151	3.106	3.197	3.178	3.470	5.041	4.739
Mn	0.053	0.105	0.102	0.000	0.051	0.000	0.060	0.049	0.353
Mg	0.530	0.670	0.590	0.435	0.449	0.432	0.455	0.673	0.496
Zn	0.000	0.000	0.000	0.093	0.136	0.191	0.000	0.000	0.000
Ca	0.000	0.000	0.000	0.000	0.000	0.000	0.000	0.354	0.587
Total	29.343	29.450	29.313	29.317	29.404	29.434	29.438	16.058	16.072
X_{Fe}	0.86	0.83	0.84	0.88	0.88	0.88	0.88	0.88	0.91
X_{Alm}								82.40	76.74
X_{Prp}								11.01	8.04
X_{Grs}								5.78	9.51
X_{Sps}								0.81	5.72

Minals (in mol%): X_{Alm} = almandine, X_{Prp} = pyrope, X_{Grs} = grossular, X_{Sps} = spessartine. X_{Fe} = Fe/(Fe+Mg); apfu = atom per formula unit; P = Panimba area, M = Mayakon area.

Muscovite is compositionally uniform in all samples, with 6.06-6.38 apfu (atoms per formula unit) Si and 0.14-0.46 apfu Na (Table 6). Muscovite from the Mayakon metapelites is slightly higher in TiO_2 (0.22-0.90 wt%) and lower in FeO (0.93-1.18 wt%) than that of the Panimba counterpart (<0.20-0.65 wt% TiO_2 and 0.73-2.32 wt% FeO). CaO and MnO are below their detection limits.

Margarite shows slight compositional variations and significant Na for Ca substitution (0.35-0.68 apfu Na, 1.35-2.57 wt% Na_2O) (Table 7). K_2O contents are >0.20 wt%, up to 0.99 wt%, in half of point analyses. Margarite is poorer in Fe than muscovite (0.23-0.69 wt% FeO); MgO, MnO and TiO_2 are below their detection limits.

Biotite chemistry is similar in all examined samples: Fe rich (X_{Fe} = 0.51-0.60) with 5.27–5.65 Si apfu and 5.70–5.99 Y (= Al^{VI} + Ti + Cr + Fe_{tot} + Mn + Mg) apfu (Table 8). The TiO_2 contents range between 1.37 and 2.29 wt%, whereas MnO is below the detection limit.

Chlorite is Fe-rich ripidolite according to Si content (5.09-5.49 apfu) and X_{Fe} value (0.56-0.75). The amount of $Al^{(IV)}$ varies between 2.52 and 2.92 apfu (Table 9). TiO_2 and MnO are generally below their detection limits, no higher than 0.37 wt% and 0.62 wt%, respectively, in chlorites from the Panimba metapelites, but are always <0.20 wt% in the Mayakon samples.

Table 6. Representative compositions of muscovite from metapelites of the Panimba and Mayakon areas. SEM EDS data (in wt%).

Area	**P**	**P**	**P**	**P**	**P**	**P**	**P**	**M**	**M**	**M**	**M**	**M**	**M**
Sample	1	2	4	4	11-a-1	21	27	39	39	45	57	60	85
SiO_2	45.93	46.85	48.44	46.42	46.25	45.61	45.93	45.70	45.83	45.97	45.65	45.48	46.25
TiO_2	<0.20	0.23	0.50	0.30	0.45	<0.20	0.65	0.58	0.35	0.43	0.43	0.22	0.90
Al_2O_3	37.30	35.26	34.22	34.60	34.18	36.43	35.56	36.05	35.92	35.94	36.90	36.60	35.81
FeO	0.73	0.94	1.63	1.81	2.32	1.52	0.85	1.16	0.99	1.18	1.03	1.03	0.93
MgO	0.28	0.71	0.53	0.58	0.91	0.25	0.70	0.51	0.60	0.55	0.35	0.41	0.56
Na_2O	1.08	0.59	0.62	0.71	0.54	0.90	0.93	1.67	1.66	0.96	1.21	0.85	1.71
K_2O	9.54	10.05	9.67	9.47	9.77	10.00	9.71	8.91	9.08	10.07	9.50	10.06	8.71
Total	94.86	94.63	95.61	93.89	94.42	94.71	94.33	94.58	94.43	95.1	95.07	94.65	94.87
Formula based on 22 oxygens, apfu													
Si	6.089	6.239	6.380	6.244	6.218	6.099	6.141	6.092	6.118	6.119	6.058	6.075	6.130
Ti	0.000	0.023	0.050	0.030	0.045	0.000	0.065	0.058	0.035	0.043	0.043	0.022	0.090
$Al^{(IV)}$	1.911	1.761	1.620	1.756	1.782	1.901	1.859	1.908	1.882	1.881	1.942	1.925	1.870
$Al^{(VI)}$	3.916	3.773	3.691	3.728	3.633	3.841	3.744	3.756	3.769	3.757	3.828	3.836	3.724
Fe^{2+}	0.081	0.105	0.180	0.204	0.261	0.170	0.095	0.129	0.111	0.131	0.114	0.115	0.103

 doi:10.20944/preprints202308.0273.v1

Mg	0.055	0.141	0.104	0.116	0.182	0.050	0.140	0.101	0.119	0.109	0.069	0.082	0.111
Na	0.278	0.152	0.158	0.185	0.141	0.233	0.241	0.432	0.430	0.248	0.311	0.220	0.439
K	1.613	1.707	1.625	1.625	1.675	1.706	1.656	1.515	1.546	1.710	1.608	1.714	1.473
Total	13.943	13.901	13.807	13.889	13.937	14.000	13.941	13.991	14.009	13.998	13.974	13.989	13.939
X_{Fe}	0.59	0.43	0.63	0.64	0.59	0.77	0.41	0.56	0.48	0.55	0.62	0.59	0.48

X_{Fe} = Fe/(Fe+Mg); apfu = atoms per formula unit; P = Panimba area, M = Mayakon area. MnO and CaO are below detection limit (<0.20 wt%).

Table 7. Representative compositions of margarite from metapelites of the Panimba and Mayakon areas. SEM EDS data (in wt%).

Area	**P**	**P**	**P**	**P**	**M**	**M**
Sample	11a	11a	11a	11a	45	57
SiO_2	31.47	28.90	34.87	30.61	32.63	30.94
Al_2O_3	50.49	52.17	46.12	51.66	47.41	49.88
FeO	0.36	0.44	0.44	0.69	0.49	0.45
CaO	10.75	10.00	7.57	10.70	9.23	11.77
Na_2O	1.82	1.67	2.82	2.13	2.52	1.35
K_2O	<0.20	<0.20	0.99	<0.20	0.43	0.24
Total	94.89	93.18	92.81	95.79	92.71	94.63
Formula based on 22 oxygens, apfu						
Si	4.176	3.907	4.703	4.041	4.429	4.138
$Al^{(IV)}$	3.824	4.093	3.297	3.959	3.571	3.862
$Al^{(VI)}$	4.073	4.220	4.034	4.078	4.013	3.999
Fe^{2+}	0.040	0.050	0.050	0.076	0.056	0.050
Ca	1.528	1.448	1.094	1.513	1.342	1.686
Na	0.468	0.438	0.737	0.545	0.663	0.350
K	0.000	0.000	0.170	0.000	0.074	0.041
Total	14.109	14.155	14.085	14.213	14.148	14.127

apfu = atoms per formula unit; P = Panimba area, M = Mayakon area. TiO_2, MnO, and MgO are below detection limit (<0.20 wt%).

Table 8. Representative compositions of biotite from metapelites of the Panimba and Mayakon areas. SEM EDS data (in wt%).

Area	**P**	**P**	**P**	**P**	**P**	**P**	**P**	**M**	**M**	**M**	**M**	**M**
Sample	4	4	10	10	27	27	27	60	60	60	60	85
SiO_2	34.42	34.14	33.87	34.61	35.15	35.02	38.21	35.26	35.34	35.64	34.74	37.59
TiO_2	1.57	1.70	1.67	1.98	1.77	1.80	1.47	2.29	2.02	2.14	1.37	1.58
Al_2O_3	20.69	20.09	20.27	19.20	19.33	19.16	19.48	19.58	19.76	18.74	20.01	19.39
FeO	22.73	22.87	22.32	21.74	20.76	20.46	20.04	21.33	21.86	19.81	20.88	18.17
MgO	8.16	8.94	7.93	7.99	9.39	9.67	9.45	8.04	8.32	10.23	9.14	9.63
K_2O	7.43	8.07	8.40	9.02	8.60	8.42	8.12	8.65	8.72	8.89	8.85	7.84
Total	95.00	95.81	94.46	94.54	95.00	94.53	96.77	95.15	96.02	95.45	94.99	94.20
Formula based on 22 oxygens, apfu												
Si	5.270	5.218	5.250	5.363	5.371	5.368	5.638	5.390	5.366	5.403	5.321	5.649
Ti	0.181	0.195	0.195	0.231	0.203	0.208	0.163	0.263	0.231	0.244	0.158	0.179
Al(IV)	2.730	2.782	2.750	2.637	2.629	2.632	2.362	2.610	2.634	2.597	2.679	2.351
Al(VI)	1.003	0.836	0.953	0.869	0.852	0.830	1.026	0.917	0.902	0.751	0.932	1.084
Fe^{2+}	2.910	2.923	2.893	2.817	2.653	2.623	2.473	2.727	2.775	2.511	2.674	2.283
Mg	1.863	2.037	1.833	1.846	2.139	2.210	2.079	1.832	1.883	2.312	2.087	2.158
K	1.451	1.573	1.661	1.783	1.676	1.646	1.528	1.687	1.689	1.719	1.729	1.503

Preprints (www.preprints.org) | NOT PEER-REVIEWED | Posted: 3 August 2023 doi:10.20944/preprints202308.0273.v1

Total	15.408	15.564	15.534	15.545	15.523	15.517	15.269	15.426	15.480	15.538	15.580	15.206
X_{Fe}	0.61	0.59	0.61	0.60	0.55	0.54	0.54	0.60	0.60	0.52	0.56	0.51

X_{Fe} = Fe/(Fe+Mg); apfu = atoms per formula unit; P = Panimba area, M = Mayakon area.

Table 9. Representative compositions of chlorite from metapelites of the Panimba and Mayakon areas. SEM EDS data (in wt%).

Area	**P**	**P**	**P**	**P**	**P**	**P**	**P**	**P**	**M**	**M**	**M**	**M**	**M**	**M**	**M**	**M**	**M**
Sample	3	10	10	11a	11a	11a	11a	11a	39	39	45	57	57	57	57	57	57
SiO_2	25.16	23.21	22.44	25.82	24.97	23.70	24.65	23.73	24.24	23.96	23.25	23.85	23.94	23.08	23.60	22.83	23.47
TiO_2	<0.20	<0.20	<0.20	<0.20	<0.20	0.37	0.35	<0.20	<0.20	<0.20	<0.20	<0.20	<0.20	<0.20	<0.20	<0.20	<0.20
Al_2O_3	22.35	22.65	18.08	22.98	22.33	21.86	21.43	21.86	21.65	22.45	22.41	21.80	21.77	22.07	22.33	21.77	21.94
Fe_2O_3*	1.46	0.07	0.00	2.27	1.70	0.37	0.68	1.12	0.00	1.01	0.23	0.06	0.10	0.13	0.10	0.00	0.04
FeO*	29.16	28.53	36.82	27.64	28.61	30.58	30.53	29.69	28.57	35.00	30.01	30.66	30.44	29.92	30.40	30.57	30.32
MnO	0.62	<0.20	<0.20	<0.20	<0.20	0.32	0.30	<0.20	<0.20	<0.20	<0.20	<0.20	<0.20	<0.20	<0.20	<0.20	<0.20
MgO	9.70	11.67	7.78	8.84	9.63	9.83	10.45	8.72	12.64	6.62	10.46	10.98	11.08	10.50	10.88	10.56	10.86
K_2O	<0.20	<0.20	0.69	0.53	<0.20	0.23	<0.20	0.14	<0.20	<0.20	<0.20	<0.20	<0.20	<0.20	<0.20	<0.20	<0.20
Total	88.46	86.13	85.81	88.08	87.24	87.26	88.40	85.26	87.10	89.04	86.36	87.35	87.33	85.70	87.31	85.73	86.62
Formula based on 28 oxygens, apfu																	
Si	5.383	5.085	5.165	5.485	5.394	5.192	5.315	5.299	5.241	5.246	5.123	5.204	5.218	5.129	5.145	5.088	5.162
Ti	0.000	0.000	0.000	0.000	0.000	0.061	0.057	0.000	0.000	0.000	0.000	0.000	0.000	0.000	0.000	0.000	0.000
$Al^{(IV)}$	2.617	2.915	2.835	2.515	2.606	2.808	2.685	2.701	2.759	2.754	2.877	2.796	2.782	2.871	2.855	2.912	2.838
$Al^{(VI)}$	3.044	2.936	2.151	3.292	3.108	2.849	2.772	3.077	2.759	3.056	2.947	2.812	2.813	2.912	2.885	2.815	2.850
Fe^{3+}	0.235	0.011	0.000	0.363	0.276	0.061	0.111	0.189	0.000	0.166	0.039	0.009	0.017	0.022	0.016	0.000	0.006
Fe^{2+}	5.219	5.227	7.441	4.910	5.169	5.602	5.506	5.545	5.166	6.409	5.530	5.595	5.548	5.561	5.543	5.739	5.576
Mn	0.112	0.000	0.000	0.000	0.000	0.059	0.055	0.000	0.000	0.000	0.000	0.000	0.000	0.000	0.000	0.000	0.000
Mg	3.094	3.811	2.669	2.800	3.101	3.210	3.359	2.903	4.074	2.161	3.436	3.572	3.600	3.478	3.536	3.508	3.560
K	0.000	0.000	0.405	0.287	0.000	0.129	0.000	0.080	0.000	0.000	0.000	0.000	0.000	0.000	0.000	0.000	0.000
Total	19.704	19.986	20.666	19.652	19.654	19.971	19.860	19.793	20.000	19.792	19.952	19.988	19.972	19.972	19.982	20.062	19.992
X_{Fe}	0.64	0.58	0.74	0.65	0.64	0.64	0.63	0.66	0.56	0.75	0.62	0.61	0.61	0.62	0.61	0.621	0.61

X_{Fe} = Fe/(Fe+Mg); apfu = atoms per formula unit; P = Panimba area, M = Mayakon area. *The contents of Fe^{3+} and Fe^{2+} are calculated stoichiometrically. CaO and Na_2O are below detection limit (<0.20 wt%).

Fe-Ti oxides are *ilmenite* and *rutile*. Ilmenite always contains notable amounts of MnO (0.96-2.13 wt%) conforming to 0.020-0.045 Mn apfu, while MgO is below detection limit. Ilmenite in samples from the contact metamorphic aureole in the Panimba area is slightly richer in MnO (3.11-4.69 wt%) than that from other samples (Table 10). Rutile is nearly pure TiO_2 with 0.36-1.20 wt% FeO.

Table 10. Representative compositions of ilmenite and rutile from metapelites of the Panimba and Mayakon areas. SEM EDS data (in wt%).

Mineral	**Ilmenite**								**Rutile**		
Area	P	P	P	P	P	M	M	M	P	M	M
Sample	4	10	11a	21	29	39	57	60	11a	39	57
SiO_2	0.39	0.30	0.32	0.45	0.24	<0.20	<0.20	0.24	<0.20	<0.20	<0.20
TiO_2	53.58	54.81	55.73	54.46	53.56	53.08	52.56	53.28	99.95	99.38	99.10
FeO	45.07	43.41	41.17	39.50	42.51	46.65	45.18	46.17	0.36	1.20	1.08
MnO	1.10	1.67	2.13	4.69	3.11	0.96	1.72	0.99	<0.20	<0.20	<0.20
Total	100.13	100.18	99.35	99.09	99.42	100.68	99.46	100.68	100.31	100.58	100.18
	Formula based on 3 oxygen, apfu								Formula based on 2 oxygen, apfu		
Si	0.010	0.007	0.008	0.011	0.006	0.000	0.000	0.006	0.000	0.000	0.000
Ti	1.008	1.024	1.042	1.026	1.014	1.001	1.003	1.001	0.998	0.993	0.994
Fe	0.942	0.902	0.856	0.827	0.894	0.978	0.958	0.965	0.004	0.013	0.012

Preprints (www.preprints.org) | NOT PEER-REVIEWED | Posted: 3 August 2023 doi:10.20944/preprints202308.0273.v1

Mn	0.023	0.035	0.045	0.099	0.066	0.020	0.037	0.021	0.000	0.000	0.000
Total	1.983	1.968	1.950	1.963	1.980	1.999	1.997	1.993	1.002	1.007	1.006

apfu = atoms per formula unit; P = Panimba area, M = Mayakon area.

Phosphate minerals include *monazite, xenotime,* and *fluorapatite*. Monazite has a composition of $(Ce_{0.31–0.48}La_{0.15–0.25}Nd_{0.13–0.18}Pr_{0.04–0.06}Th_{0.02–0.26}Ca_{0.01–0.10}Sm_{0.02–0.04}Gd_{0.00–0.02}U_{0.00–0.01})PO_4$ (Table 11). All grains contain Ca (0.22–2.35 wt% CaO) and some also contain up to 0.99 wt% UO_2. Monazite shows large ranges of Th: ThO_2 varies from 1.2 to 19.16 wt% in the Mayakon samples and does not exceed 5.84 wt% in the Panimba ones. Data on tiny grains of xenotime are restricted to relative contents of cations: Y >> Dy ≈ Er ≈ Yb > Gd > Ho> Tm. Fluorapatite lacks sulfate sulfur and chlorine but some grains contain appreciable amounts of Si (up to 0.53 wt% SiO_2) (Table 11).

Fe and Cu sulfides include *pyrite, pyrrhotite, chalcopyrite* and *cubanite* (Table 12). Pyrite is close to its theoretical formula, with $Fe_{0.97-1.02}Ni_{0.00-0.02}S_2$. Few point analyses yielded >0.20 wt% Ni, with a maximum of 1.17 wt%. Other impurities are below their detection limits. Many pyrite grains are partly replaced by Fe^{3+}-(oxy)hydroxides (Table 12) which adsorb notable amounts of Co (up to 1.1 wt%), Ni (up to 3.4 wt%), and Cu (up to 1.2 wt%). The formula of pyrrhotite covers a narrow range of $Fe_{0.87–0.92}S_1$. All other elements are below their detection limits. The compositional ranges of chalcopyrite ($Cu_{0.99–1.00}Fe_{1.00–1.03}S_2$) and cubanite ($Cu_{0.99}Fe_{2.01}S_3$) are close to the ideal stoichiometry. Fine (<1 μm) grains of molibdenite, galena, as well as Ag, Bi and Te sulfides are too small for precise analysis of mineral chemistry.

Table 11. Representative compositions of monazite and fluorapatite from metapelites of the Panimba and Mayakon areas. SEM EDS data (in wt%).

Mineral	**Monazite**						**Fluorapatite**	
Area	P	P	P	M	M	M	M	M
Sample	1	10	27	57	60	85	60	60
CaO	0.42	0.97	0.46	1.44	0.32	1.80	55.21	54.79
La_2O_3	15.93	14.71	15.16	13.38	17.15	10.98	<0.20	<0.20
Ce_2O_3	32.07	28.29	29.38	27.84	31.10	23.71	<0.20	<0.20
Pr_2O_3	2.83	3.69	3.00	3.56	3.32	2.90	<0.20	<0.20
Nd_2O_3	10.49	11.57	11.40	11.03	11.13	9.70	<0.20	<0.20
Sm_2O_3	1.97	1.70	1.37	2.31	2.41	1.69	<0.20	<0.20
Gd_2O_3	1.68	1.68	1.38	1.50	1.46	1.59	<0.20	<0.20
ThO_2	2.34	5.67	5.84	8.30	2.20	19.16	<0.20	<0.20
UO_2	0.75	0.66	<0.20	<0.20	0.33	<0.20	<0.20	<0.20
P_2O_5	30.91	30.15	30.43	30.36	30.45	27.54	42.54	42.67
SiO_2	<0.20	<0.20	<0.20	<0.20	<0.20	<0.20	<0.20	0.34
F	<0.20	<0.20	<0.20	<0.20	<0.20	<0.20	3.99	4.28
Total							101.74	102.08
$O-(F,Cl)_2$							1.68	1.80
Total	99.39	99.09	98.42	99.72	99.87	99.07	100.06	100.28
Formula based on			4 oxygen, apfu				10 cations, apfu	
Ca	0.017	0.040	0.019	0.059	0.013	0.076	10.000	10.000
La	0.227	0.211	0.218	0.190	0.246	0.161	0.000	0.000
Ce	0.454	0.403	0.420	0.392	0.443	0.344	0.000	0.000
Pr	0.040	0.052	0.043	0.050	0.047	0.042	0.000	0.000
Nd	0.145	0.161	0.159	0.152	0.155	0.137	0.000	0.000
Sm	0.026	0.023	0.018	0.031	0.032	0.023	0.000	0.000
Gd	0.022	0.022	0.018	0.019	0.019	0.021	0.000	0.000
Th	0.031	0.075	0.078	0.109	0.029	0.259	0.000	0.000
U	0.010	0.009	0.000	0.000	0.005	0.000	0.000	0.000
P	1.012	0.993	1.005	0.989	1.003	0.925	6.083	6.148

 doi:10.20944/preprints202308.0273.v1

Si	0.000	0.000	0.000	0.000	0.000	0.000	0.000	0.058
F	0.000	0.000	0.000	0.000	0.000	0.000	2.131	2.304

apfu = atoms per formula unit; P = Panimba area, M = Mayakon area.

Table 12. Representative compositions of sulphides from metapelites of the Panimba and Mayakon areas. SEM EDS data (in wt%).

Mineral	**Pyrrhotite**			**Pyrite**			**Chalcopyrite**		**Cubanite**
Area	P	P	M	P	P	P	P	P	P
Sample	4	27	60	21	21	29	27	29	21
Fe	60.70	59.87	60.74	46.42	47.17	46.06	30.9	30.58	41.23
Cu	<0.20	<0.20	<0.20	<0.20	<0.20	<0.20	34.01	34.27	23.21
S	38.05	39.29	38.45	53.08	52.92	52.80	34.38	34.80	35.32
Total	99.02	99.16	99.19	99.50	100.09	98.86	99.29	99.65	99.76
Formula based on	1 sulphur, apfu			2 sulphur, apfu			2 sulphur, apfu		3 sulphur, apfu
Fe	0.916	0.875	0.907	1.004	1.023	1.002	1.032	1.009	2.010
Cu	0.000	0.000	0.000	0.000	0.000	0.000	0.998	0.994	0.995
Total	0.916	0.875	0.907	1.004	1.023	1.002	2.030	2.003	3.005

apfu = atoms per formula unit; P = Panimba area, M = Mayakon area.

4.2. Mineralogy and Chemistry of Concentrates from Al-Rich Metapelites

The concentrates of andalusite and kyanite were extracted in laboratory from six representative samples of high-alumina metapelites. They were andalusite concentrates from the Panimba samples (Nos. 10, 28, 30), kyanite concentrates from both Panimba (27) and Mayakon (70) samples, and mixed andalusite-kyanite from Mayakon sample 36a. Mainly andalusitic rocks contained 14-17 wt% andalusite, 49-55 wt% quartz, 21 to 29 wt% micas (muscovite + biotite ± margarite), 1 to 7 wt% chlorite, within 5 wt% staurolite, 4 wt% K-feldspar, and 2 wt% kyanite. The mineralogy of mainly kyanitic rocks included 13-20 wt% kyanite, 45-50 wt% quartz, 9 to 24 wt% micas (muscovite + biotite ± margarite), within 15 wt% chlorite, 14 wt% staurolite, 8 wt% plagioclase, and 5 wt% andalusite. The rocks were crushed, milled, and screened to grain size fractions <0.06, 0.06≤x<0.1, and 0.1≤x<0.25 mm; 11-14 wt% and 43-55 wt% yields of the fractions 0.06≤x<0.1 and 0.1≤x<0.25 mm were used to obtain Al_2SiO_5 concentrates.

Tailings (<0.06 mm), reaching a yield of 32-44 wt%, consisted of quartz (50-68 wt%), micas (16-27 wt%), staurolite (5-15 wt%), chlorite (up to 11 wt%), and plagioclase (up to 14 wt%). The losses were 3-11 wt% for andalusite and within 3 wt% for kyanite. The major-element contents of tailings were comparable with those in bulk rock samples, while the enrichment in some trace elements bound in accessory micrograins (≤ 10 μm) was higher: 81.3-150 ppm Zr, 4.92-15.9 ppm Th, 1.78-3.04 ppm U, and 65.5-252 ppm ΣREE.

The yield of *magnetic product* was 4-8 wt% and 26-41 wt% for the 0.06-0.1 mm and 0.1-0.25 mm fractions, respectively. Magnetic product, carrier of Fe-bearing minerals, included up to 56 wt% staurolite, 43 wt% biotite, 18 wt% chlorite, ilmenite, and sulfides (Figure 11). Compared to the initial samples, the magnetic product showed 2-4 times greater enrichment in Fe_2O_3 (15.18-19.15 wt%), TiO_2 (1.29-2.12 wt%), V (110-290 ppm), Cr (100-270 ppm), Co (15-50 ppm), Ni (23-80 ppm), and Cu (29-120 ppm).

Preprints (www.preprints.org) | NOT PEER-REVIEWED | Posted: 3 August 2023 doi:10.20944/preprints202308.0273.v1

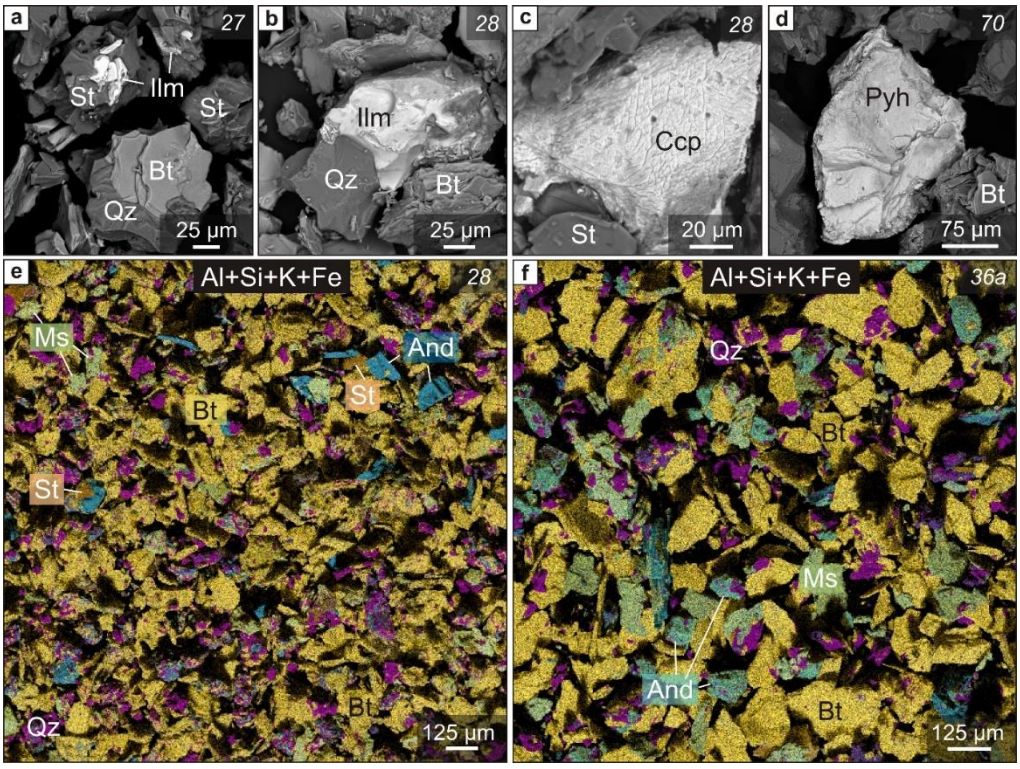

Figure 11. Mineralogy of magnetic product (step 1) extracted from Fe- and Al-rich metapelites of the Teya metamorphic complex. Magnetic product contains predominant biotite and lesser amounts of muscovite, staurolite, ilmenite, and sulfides. Back-scattered images (**a-d**) and multi-element maps (Al, Si, K, and Fe) (**e, f**). And = andalusite, Bt = biotite, Ccp = chalcopyrite, Ilm = ilmenite, Ms = muscovite, Pyh = pyrrhotite, Qz = quartz, St = staurolite. Numerals in top right corner of panels are sample numbers.

Grains of biotite and sulfides, as well as the largest ilmenite grains, were completely isolated, while staurolite and fine ilmenite grains remained intergrown with quartz (Figure 11a-d). Incomplete isolation of andalusite led to 2-10 wt% losses of the economic component: andalusite remained intergrown with biotite, quartz, and staurolite in the magnetic product (Figure 11e,f), while the losses of kyanite were within 3 wt%.

Light product consisted of quartz (67 to 91 wt%), feldspar (up to 21 wt%), and white micas (5 to 21 wt%) (Figure 12). The grains of these minerals were mostly isolated from the intergrowths to separate particles (Figure 12a,b). The light product contained more SiO_2 (70.09-85.21 wt%) and Ba (240-1100 ppm) than the initial samples and had moderate contents of K_2O (1.17-4.06 wt%) and Na_2O (within 1.97 wt%). The yield of light product from andalusite samples was 3 to 11 wt%. The losses of the andalusite economic component were 6-8 wt% from the 0.1-0.25 mm fractions and up to 19-23 wt% from the 0.06-0.1 mm fractions (Figure 12d). For the kyanite samples, the yield values were 6-9 wt% (0.06-0.1 mm) and 7 to 25 wt% (0.1-0.25 mm), at ≤ 3 wt% losses (Figure 12c).

Preprints (www.preprints.org) | NOT PEER-REVIEWED | Posted: 3 August 2023 doi:10.20944/preprints202308.0273.v1

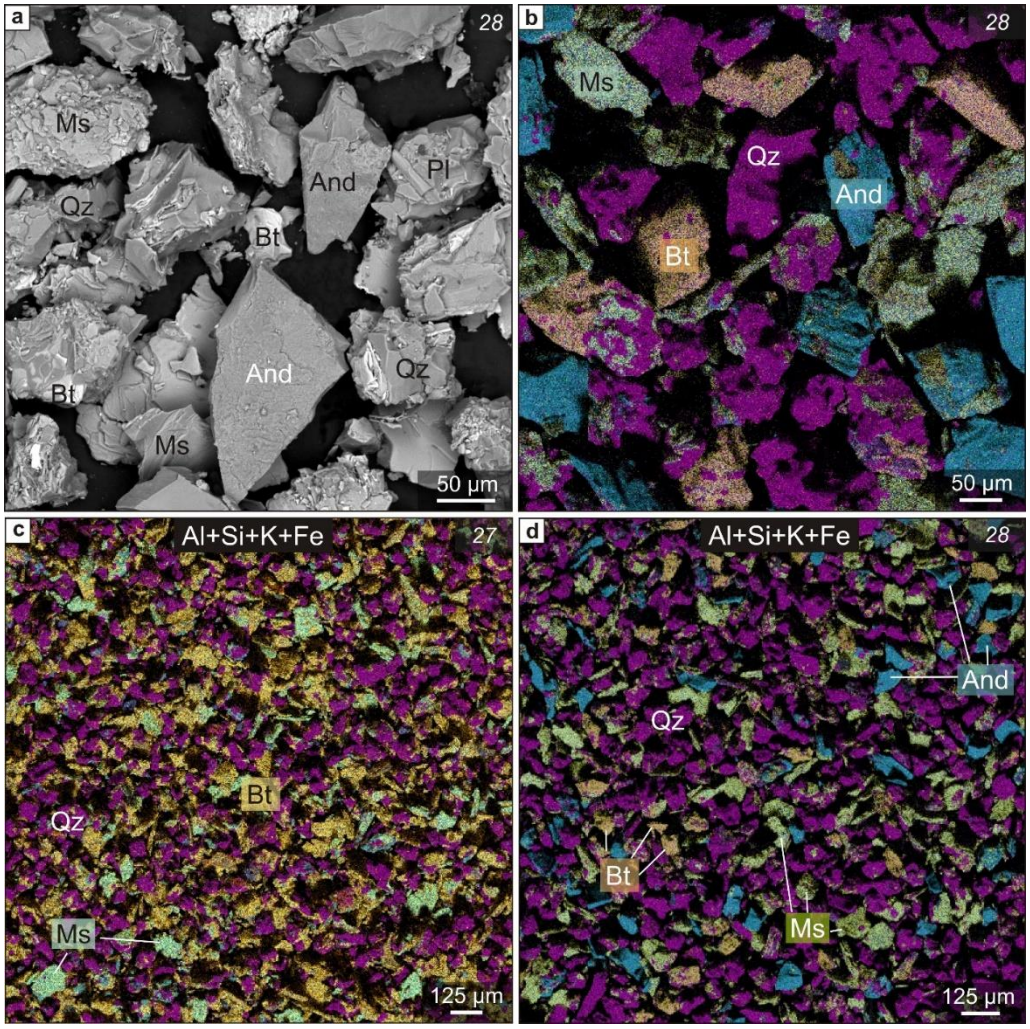

Figure 12. Mineralogy of light product (step 2) extracted from Fe-Al metapelites of the Teya metamorphic complex. Light product contains predominant quartz and muscovite and lesser amounts of biotite. Back-scattered image (**a**) and multi-element maps (Al, Si, K, and Fe) (**b-d**). And = andalusite, Bt = biotite, Ms = muscovite, Pl = plagioclase, Qz = quartz. Numerals in top right corner of panels are sample numbers.

Raw Al_2SiO_5 concentrate contained moderate amounts of partly isolated quartz (1-25 wt%), micas (2-19 wt%), staurolite (1-12 wt%), and chlorite (≤4 wt%) grains (Figures 13 and 14). The contents of Al_2O_3 reached 43.92-54.05 wt%, while impurities were low: TiO_2 (0.27-1.31 wt%) and K_2O (0.83-2.25 wt%), as well as V (30-110 ppm), Co (2.1-25 ppm), and Ni (5-60 ppm). Ferric iron was within 1.71-4.96 wt% in most of the concentrate samples, except for sample 36a where it reached 6.97 wt% Fe_2O_3 due to the presence of biotite and Fe-rich chlorite (up to 19 wt% and 12 wt%, respectively). The greatest amount of andalusite (78-79 wt%) was extracted from the coarse fraction (0.1-0.25 mm) where it quite often remained intergrown with quartz and micas (Figure 13a-d). The 0.06-0.1 mm fractions yielded 60-69 wt% andalusite, but its grains were more often isolated, with rare intergrowths (Figure 13e). Kyanite varied from 52 wt% to 92 wt% and occurred mostly as isolated plates (Figure 14). Grains of both Al_2SiO_5 polymorphs enclosed fine (10-50 μm) micas, quartz, and accessories, especially ilmenite (Figures 13a-c and 14a-c). The yield of andalusite raw concentrate was 2.9-5.4 wt% for the 0.1-0.25 mm fraction and 0.1-0.5 wt% for the 0.06-0.1 mm fraction. The respective values for the kyanite raw concentrate were 1.2-2.0 wt% (0.1-0.25 mm) and 0.1-0.4 wt% (0.06-0.1 mm).

Preprints (www.preprints.org) | NOT PEER-REVIEWED | Posted: 3 August 2023 doi:10.20944/preprints202308.0273.v1

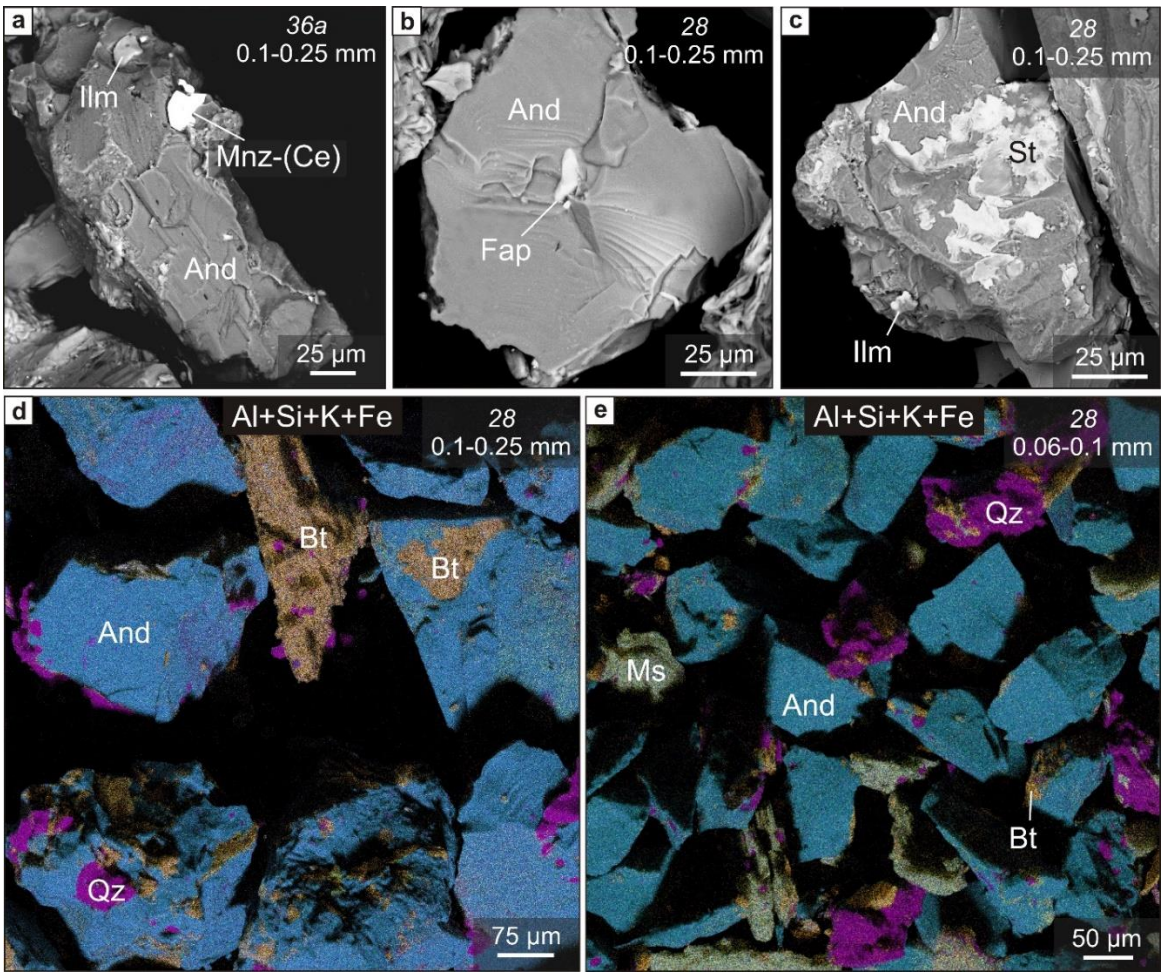

Figure 13. Mineralogy of raw andalusite concentrate (step 3) obtained from Fe-Al metapelites of the Teya metamorphic complex: (**a, b**) Ilmenite, fluorapatite and monazite inclusions in andalusite; (**c**) Intergrown andalusite and staurolite; (**d, e**) Main phases in raw andalusite concentrate, different grain sizes. Andalusite is partly separated. Back-scattered images (a-c) and multi-element maps (Al, Si, K, and Fe) (d, e). And = andalusite, Bt = biotite, Fap = fluorapatite, Ilm = ilmenite, Mnz-Ce = monazite-Ce, Ms = muscovite, Qz = quartz, St = staurolite. Numerals in top right corner of panels are sample numbers (above) and grain sizes (below).

Preprints (www.preprints.org) | NOT PEER-REVIEWED | Posted: 3 August 2023 doi:10.20944/preprints202308.0273.v1

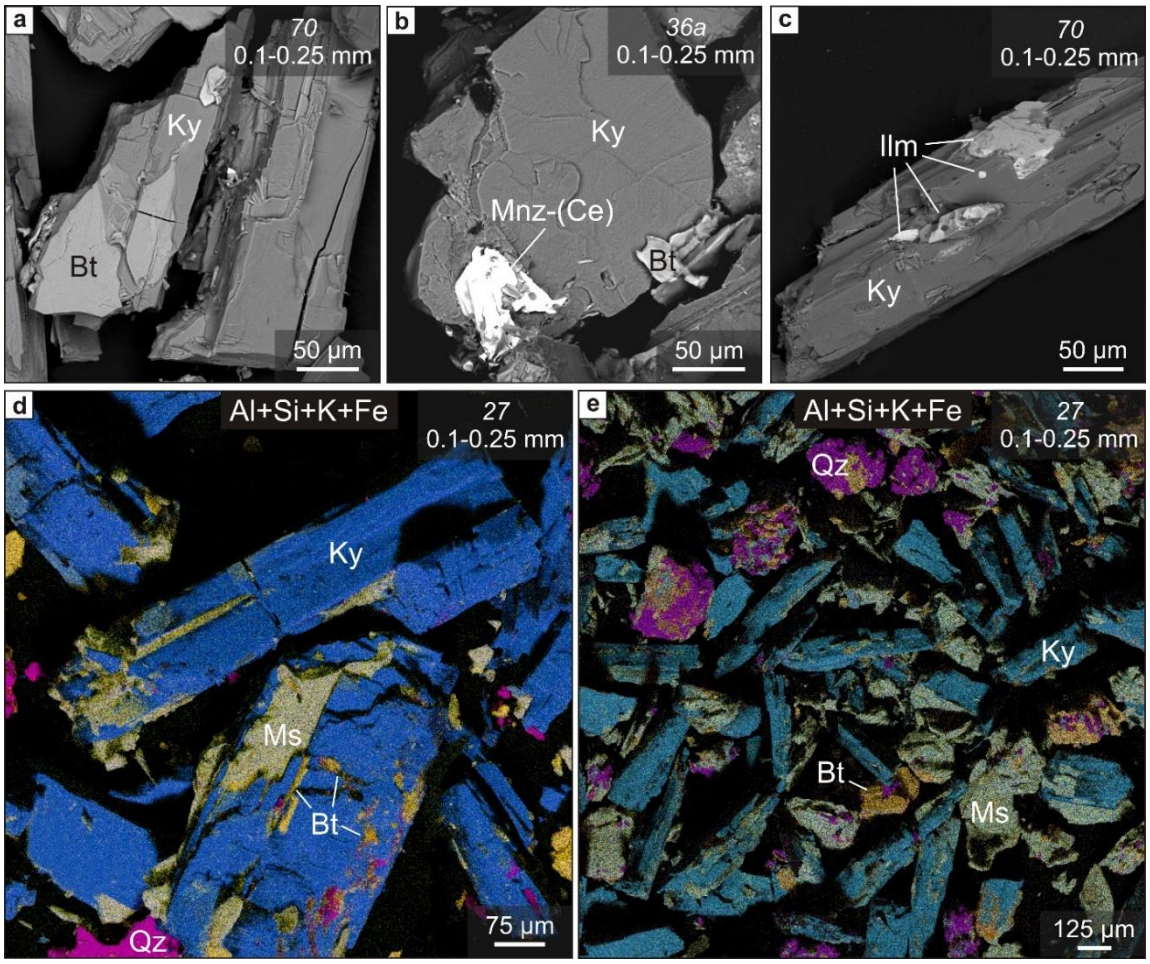

Figure 14. Mineralogy of raw kyanite concentrate (step 3) obtained from Fe-Al metapelites of the Teya metamorphic complex: (**a-c**) Biotite, ilmenite and monazite inclusions in kyanite; (**c**) Intergrown kyanite, muscovite, and biotite; (**e**) Main phases in raw kyanite concentrate, different grain sizes. Kyanite is partly liberated. Back-scattered images (a-c) and multi-element maps (Al, Si, K, and Fe) (d, e). Bt = biotite, Ilm = ilmenite, Ky = kyanite, Mnz-Ce = monazite-Ce, Ms = muscovite, Qz = quartz. Numerals in top right corner of panels are sample numbers (above) and grain sizes (below).

Final Al_2SiO_5 concentrate contained 70-95 wt% and 73-97 wt% Al_2SiO_5 in the 0.1-0.25 mm and 0.06-0.1 mm fractions, respectively, with the yield 0.7-4.1 wt% (0.1-0.25 mm) and 0.1-0.6 wt% (0.06-0.1 mm). Staurolite and sulfides were removed from the final product, and only small amounts of quartz and micas (3-9 wt% and 2-12 wt%, respectively) generally remained, except for 21-23 wt% quartz in the concentrate from samples 10 and 28 (0.06-0.1 mm) and 30 wt% mica in that of sample 70, fraction 0.1-0.25 mm (Figures 15 and 16). The final concentrate of sample 36a still contained 7-12 wt% chlorite. The enrichment in Al_2O_3 was three times greater than in the initial samples: 49.10-59.68 wt% and 53.82-61.40 wt% Al_2O_3 in the 0.1-0.25 mm and 0.06-0.1 mm fractions, respectively. The contents of other elements were low in the concentrate of almost all samples (0.45-0.73 wt% Fe_2O_3, 0.05-0.08 wt% TiO_2, 0.16-1.10 wt% K_2O, 11-60 ppm V, 0.7-10 ppm Co, 1.8-33 ppm Ni, 3.4-34 ppm Cu, 0.21-3.9 ppm Nb, 15-96 ppm Zr, 0.12-9 ppm Th, and 0.23-1.7 ppm U), except for 2.65-3.92 wt% Fe_2O_3 in that from chlorite-rich sample 36a. Most of andalusites enclosed ≤10 to 80 μm grains of other minerals: commonly micas, quartz, ilmenite, and monazite (Figure 15c), less frequent zircon and xenotime (Figure 15a), as well as staurolite in one sample (Figure 15b). The fewer inclusions in kyanite were most often muscovite and more rarely biotite and ilmenite (Figure 16a-c). The separation of Al_2SiO_5 intergrowths was the most complete in concentrate from the 0.06-0.1 mm fraction.

Preprints (www.preprints.org) | NOT PEER-REVIEWED | Posted: 3 August 2023 doi:10.20944/preprints202308.0273.v1

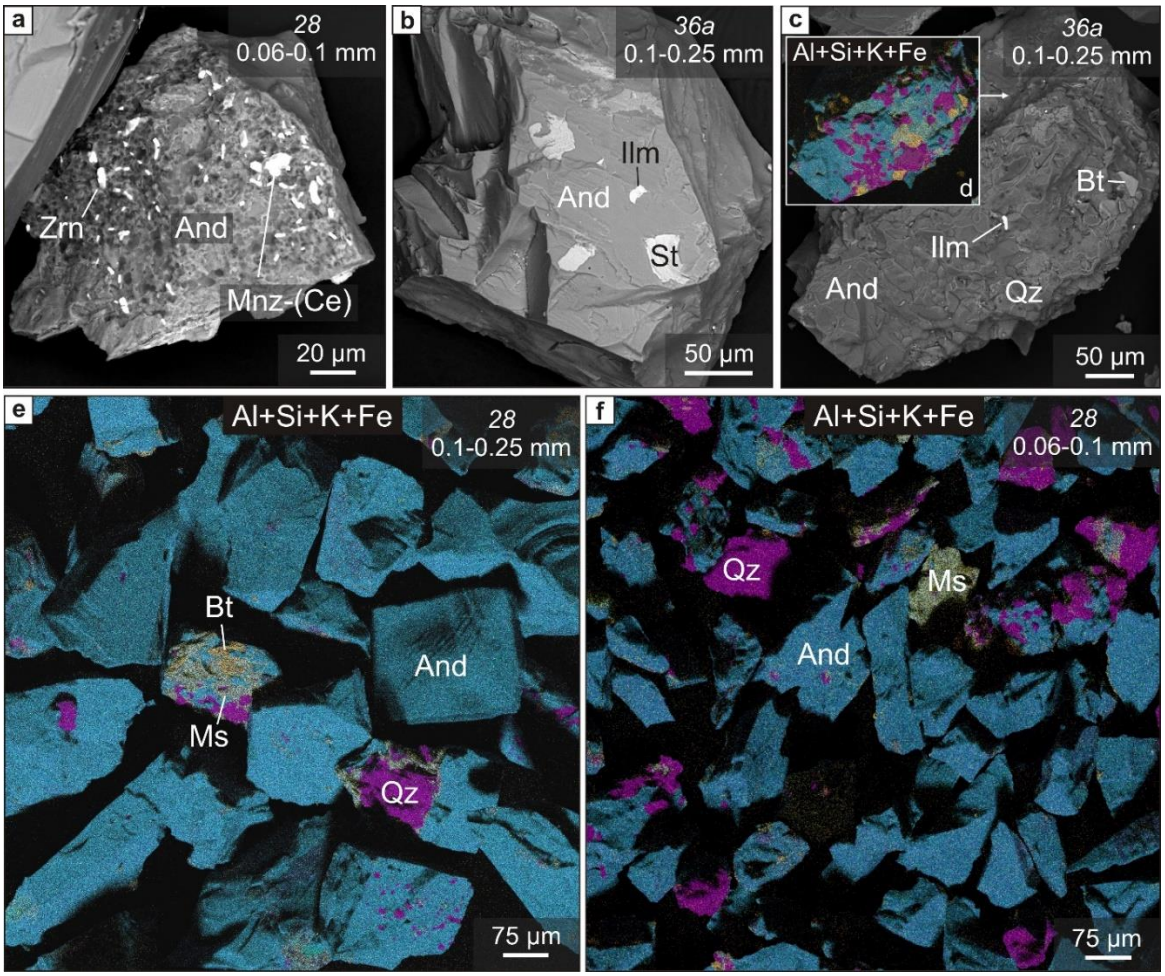

Figure 15. Mineralogy of final andalusite concentrate (step 3) obtained from Fe- and Al-rich metapelites of the Teya metamorphic complex: (**a**) Andalusite stuffed with micrograins of zircon and monazite; (**b**) Ilmenite and staurolite inclusions in andalusite; (**c, d**) Intergrown andalusite, quartz, biotite, and ilmenite; (**e, f**) Main phases in raw andalusite concentrates, different grain size. Andalusite retains quartz and mica inclusions. Back-scattered images (a-c) and multi-element maps (Al, Si, K, and Fe) (d-f). And = andalusite, Bt = biotite, Ilm = ilmenite, Mnz-Ce = monazite-Ce, Ms = muscovite, Qz = quartz, St = staurolite, Zrn = zircon. Numerals in top right corner of panels are sample numbers (above) and grain sizes (below).

Preprints (www.preprints.org) | NOT PEER-REVIEWED | Posted: 3 August 2023 doi:10.20944/preprints202308.0273.v1

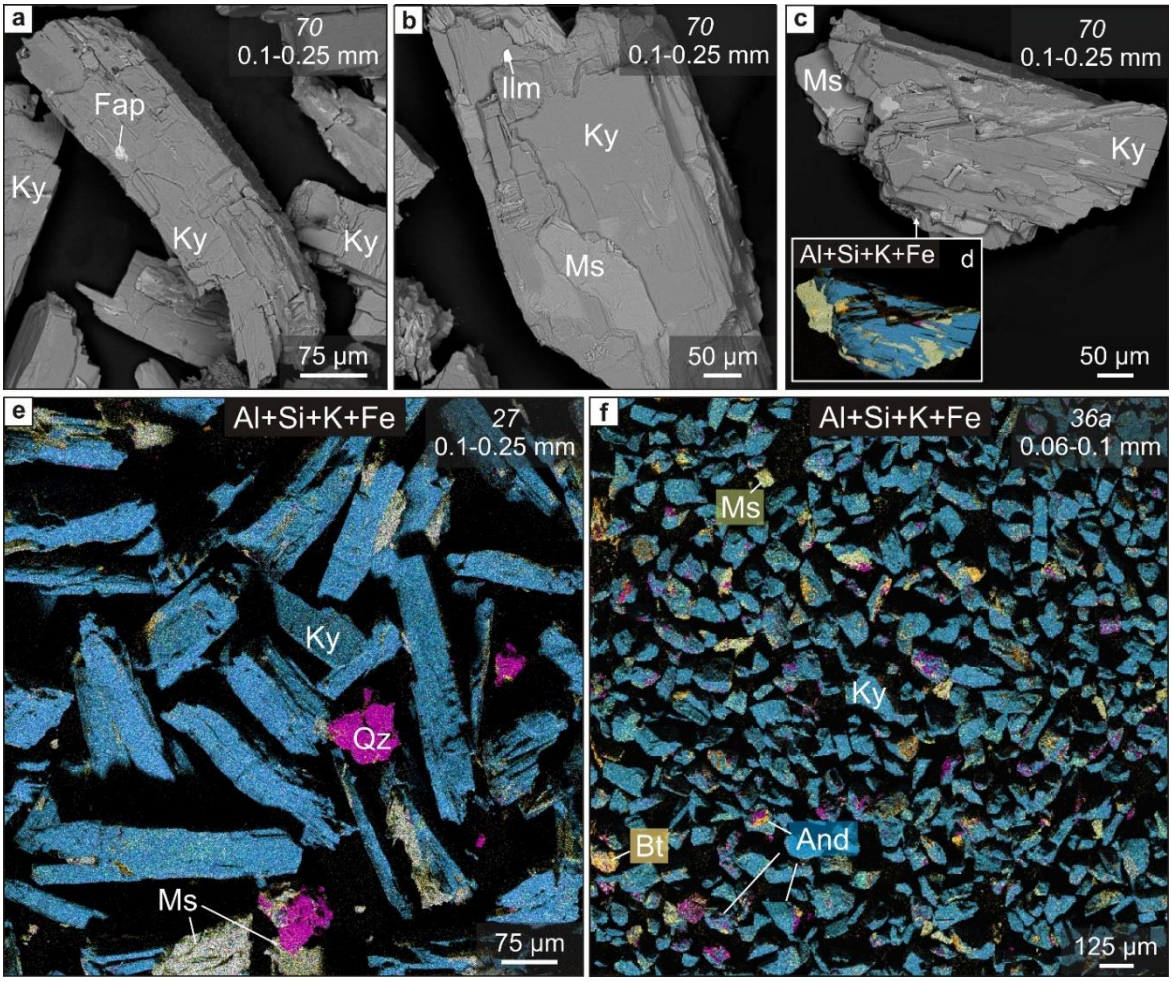

Figure 16. Mineral composition of final kyanite concentrate (step 3) obtained from Fe- and Al-rich metapelites of the Teya metamorphic complex: (**a,b**) Fluorapatite and ilmenite microinclusions in kyanite; (**c,d**) Intergrown kyanite, muscovite, and biotite; (**e,f**) Main phases in final kyanite concentrate, different grain sizes. Kyanite is mostly separated. Bt = biotite, Fap = fluorapatite, Ilm = ilmenite, Ky = kyanite, Ms = muscovite, Qz = quartz. Back-scattered images (a-c) and multi-element maps (Al, Si, K, and Fe) (d-f). Numerals in top right corner of panels are sample numbers (above) and grain sizes (below).

The mineralogy and chemistry of initial rock and concentrate samples were compared for two representative samples of andalusite-bearing (sample 28) and kyanite-bearing (sample 70) metapelites from the Teya metamorphic complex (Figures 17 and 18). Sample 28 initially contained 17 wt% andalusite, 49 wt% quartz, 24 wt% micas (muscovite + biotite ± margarite), 5 wt% staurolite, and 4 wt% K-feldspar (Figure 17). The respective mineral percentages in tailings were: andalusite 11 wt%, 60 wt% quartz, 19 wt% micas, 5 wt% staurolite, and 3 wt% chlorite. The magnetic product accumulated Fe-rich minerals: micas (25-31 wt%), staurolite (5-6 wt%), and chlorite (1-2 wt%), with quite a small loss of andalusite (5-7 wt%). The light product mainly consisted of quartz (72-73 wt%), white micas (7-12 wt%), and K-feldspar (up to 12 wt%), at andalusite losses of 6 wt% and 21 wt% from the 0.1-0.25 mm and 0.06-0.1 mm fractions, respectively. The raw Al_2SiO_5 concentrate contained 69-79 wt% andalusite, while the percentages of other minerals were within 25 wt% quartz and 9 wt% mica and chlorite. The percentages of andalusite in the final Al_2SiO_5 concentrate reached 76-92 wt%, at 6 to 21 wt% quartz and 3-2 wt% aluminosilicates.

Preprints (www.preprints.org) | NOT PEER-REVIEWED | Posted: 3 August 2023 doi:10.20944/preprints202308.0273.v1

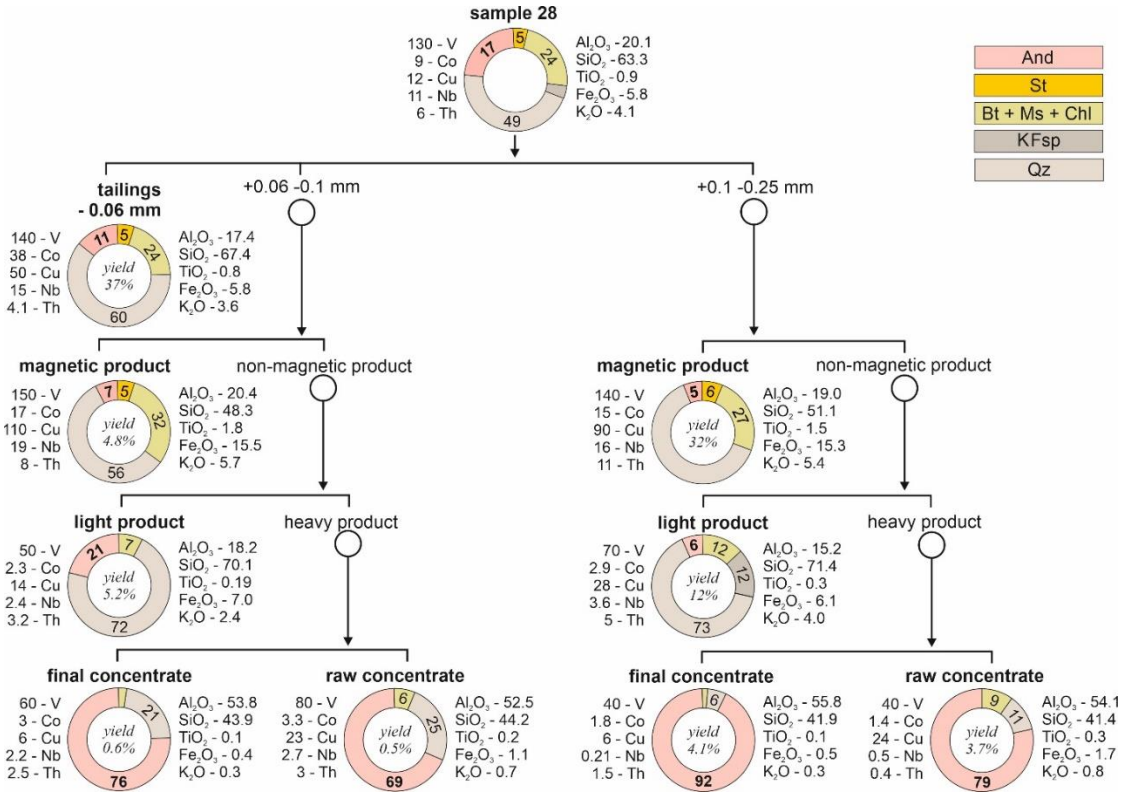

Figure 17. Phase (wt%), major-element (wt%), and trace-element (ppm) compositions of concentrates from andalusite-bearing rocks of the Teya metamorphic complex (Panimba area, sample 28). Circular diagrams show relative percentages of phases in bulk rock and concentrate samples. And = andalusite, Bt = biotite, Chl = chlorite, KFsp = potassium feldspar, Ms = muscovite, Qz = quartz, St = staurolite.

Sample 70 initially contained 5 wt% kyanite, 49 wt% quartz, 27 wt% micas (muscovite + biotite), 14 wt% staurolite, and less than 1 wt% chlorite (Figure 18). The composition of tailings was 53 wt% quartz, 27 wt% micas, 11 wt% chlorite, and 7 wt% staurolite. 44-56 wt% staurolite, and 24-35 wt% mica and chlorite were separated into the magnetic product while 73-83 wt% quartz and 14-27 wt% white micas were separated into the light product. As a result, raw Al_2SiO_5 concentrates contained 75-90 wt% kyanite at only ≤4 wt% staurolite, within 4 wt% mica and chlorite, and 3 wt% quartz. Final Al_2SiO_5 concentrate contained 70 wt% kyanite and 30% aluminosilicates, but 97 wt% kyanite and only 3 wt% quartz and aluminosilicates in the 0.1-0.25 mm and 0.06-0.1 mm fractions, respectively.

Preprints (www.preprints.org) | NOT PEER-REVIEWED | Posted: 3 August 2023 doi:10.20944/preprints202308.0273.v1

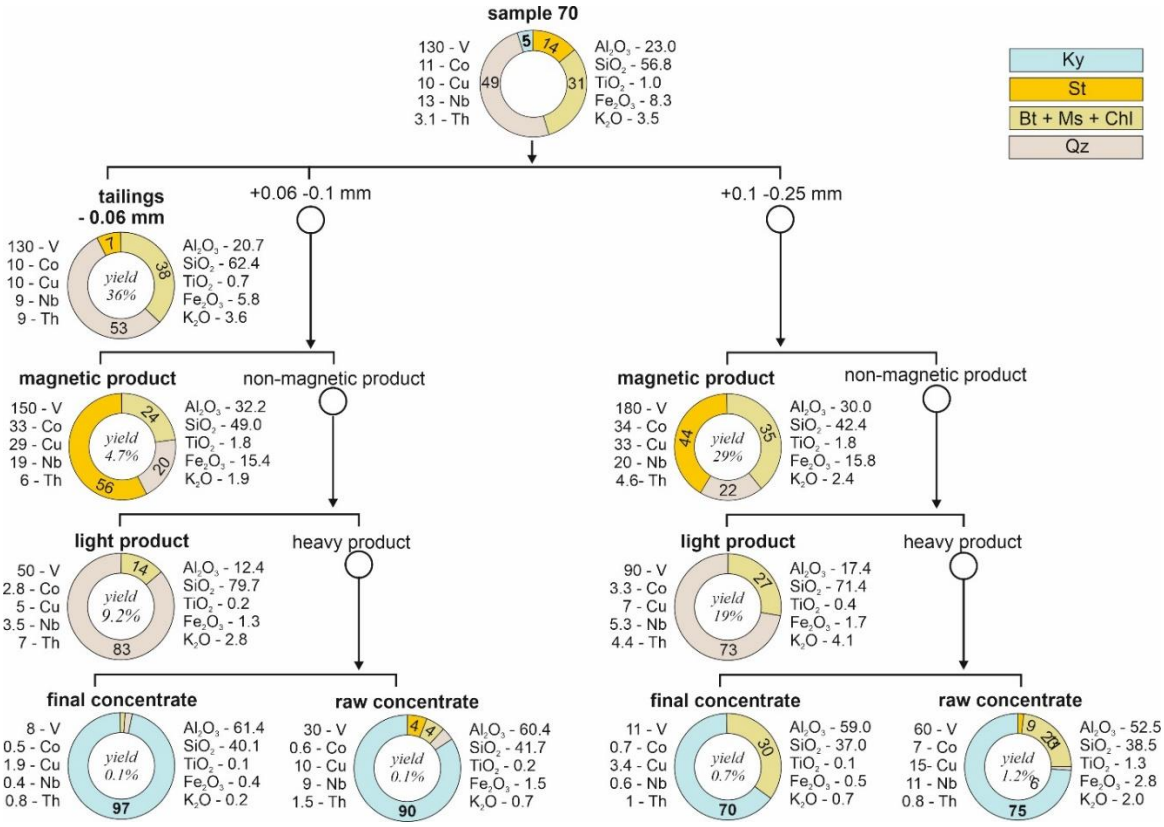

Figure 18. Phase (wt%), major-element (wt%), and trace-element (ppm) compositions of concentrates from kyanite-bearing rocks of the Teya metamorphic complex (Mayakon area, sample 70). Circular diagrams show relative percentages of phases in bulk rock and concentrate. Bt = biotite, Chl = chlorite, Ky = kyanite, Ms = muscovite, Qz = quartz, St = staurolite.

5. Discussion

5.1. High-Al Metamorphic Rocks: Resources in East Siberia

High-Al metamorphic rocks which store Al_2O_3 mainly as Al_2SiO_5 polymorphs are typical of Precambrian terrains worldwide. They commonly belong to rock complexes of Precambrian shields or microcontinents. The formation of high-grade Al_2SiO_5 ores of simple sillimanite or kyanite quartzite compositions have been traditionally interpreted as resulting from acidic leaching of polymineral metamorphic protoliths [2,47].

Deposits of sillimanite-group minerals (SGM) are currently mined in South Africa, United States of America, India, Brazil, Finland, and Spain. Kyanite and sillimanite are predominant target products (~700-750 × 10^3 tons per year), while the share of andalusite is insignificant and its deposits are rare [11]. The mining is mainly by open-pit operations, from relatively small deposits with ≥10 % SGM in the ore; the annual production is within 5 to 50× 10^3 tons of concentrate. The ore concentrate is commonly obtained through a multi-stage process including heavy-media, magnetic, and electric separation and flotation [1,2,11,48].

Russia has world richest SGM resources (~4× 10^9 tons) but no deposits have been in operation yet. Meanwhile, SGM concentrate is in large demand: ~300 × 10^3 tons yearly (as of 2010) for refractory use only [48]. Russia's richest and best documented deposits of high-Al (mainly kyanite) rocks are located in Karelia and Kola Peninsula (northwestern Russia). They are advantageous by being suitable for open-pit mining and high potential production rates. Unlike the Siberian deposits, those from northwestern Russia have been studied for three recent decades, and the dressing technology has been developed. However, most of deposits in those areas are located quite far from consumers, especially, the Keivy giant deposits which store more than 90 % of the proven kyanite resources of Russia (in total, more than 1× 10^9 tons of ore and ~340 × 10^6 tons of kyanite) [1; 2; 48].

 doi:10.20944/preprints202308.0273.v1

Numerous high-Al ore occurrences were discovered in the Urals in the 1900s [1; 48]. However, exploration and evaluation have been completed only for the small but rich Karabash deposit (15 × 10^6 tons of ore), as well as for the Andrey-Yulievo placers in the Plast district of the Chelyabinsk region [1]. All ore occurrences in the South and Central Urals are located in developed populated areas with good infrastructure and roadways and are thus promising candidates for pilot projects of SGM production in Russia [9; 48].

East Siberia possesses all principal facilities of alumina production, as well as numerous deposits and occurrences of SGM ores, mainly kyanite and sillimanite, quartzites, schists, and gneisses. However, most of them lie in hardly accessible inhabitable or scarcely populated areas. The largest deposits and occurrences of compositionally simple rich ores (e.g., sillimanite deposits of Kyakhta in Buryatia, Kitoy in the Irkutsk region, and Bazybay in the Krasnoyarsk region) were explored and evaluated in the 1950-1970s, and laboratory or pilot dressing workflows have been elaborated [1,8,48,49].

The Kyakhta sillimanite deposite can be ranked number one among the listed Siberian deposits and occurrences of high-Al rocks as to the combination of exploration and mining conditions. It is located in southwestern Buryatia not far from the Moscow-Beijing railroad and the Ulan-Ude – Kyakhta – Naushki motor road. The prospecting surveys of 1955-1959 revealed twenty ore occurrences, among which the Chernaya Sopka (Black Hill) site stores ~ 4.2 × 10^6 tons of ore in orebodies of continuous 8.5-13.5 m thickness. The ores have a simple phase composition of ~ 95 % sillimanite/fibrolite and quartz + pyrite, muscovite, and rutile, with up to 22 wt% of sillimanite on average. Sillimanite is extracted using several successive procedures: deslurrying, heavy-media separation, and flotation. The concentrate with 53.4 wt % Al_2O_3 was obtained [49]. The Kitoi and Bazybay sillimanite deposits have second highest potential, but mining and dressing will require building new roads and production facilities [1,8,49].

Rich ore occurrences with total inferred resources of 740 × 10^6 tons SGM were discovered and explored in the 1970-1980s within the Sangilen highlands (Tyva Republic). Three out of four mapped rich Sil-And-Ky occurrences are located relatively close to the Erzin – Kyzyl motor road and to the large Tes-Khem River, but the railway is about 500 km far [1; 49]. Nevertheless, the Sangilen SGM occurrences were considered [1,49] to be most favorable for large-scale production of SGM concentrates in Siberia.

5.2. High-Al Resources of Transangaria

The Yenisey Ridge territory east of the Angara River (Transangaria) is another region in Siberia where large fields of high-Al metamorphic rocks with economic average Al_2O_3 contents (~ 20 wt %; Table 1) were discovered in the second half of the 20th century. The surveys revealed about forty deposits and occurrences of kyanite-sillimanite-andalusite ores, as well as Upper Neoproterozoic rocks of the Tungusik and Oslyanka Groups with up to 20-30 % of chloritoid ($(Fe^{2+},Mg,Mn^{2+})Al_2(SiO_4)O(OH)_2$).

The high-Al rocks of the Teya complex locally have chemistry and mineralogy suitable for production of medium- and high-grade SGM concentrates. The And- and Ky-bearing rocks of the Panimba and Mayakon areas have Al_2O_3/SiO_2 ratios typical of such material and approach the Keivy Fm. kyanite-bearing schists. The varieties with highest Al_2O_3 contents (up to 24-33 wt %) are comparable with kyanite ores of the Khizovaara deposit in Karelia [2]. The amounts of $Fe_2O_{3\,tot}$ in the Teya rocks are quite high (up to 10.92 wt %, 5.83 wt % on average) but fall within the same range as in the ores of Karelia and Urals. Meanwhile the average contents of MgO (1.98 wt %) are ten times higher than in other similar deposits and occurrences of Russia (0.17-0.29 wt %) [48]. The rocks of the Yenisey Ridge store iron and magnesium mainly in abundant staurolite and biotite, and locally also in Fe-rich chlorite in zones of superimposed metamorphism.

The Teya metapelite rocks make an especially advantageous raw material for ore dressing due to vanishing contents of sulfides (SO_3 < 0.03 wt %), especially pyrite, which commonly require costly multi-stage flotation to remove [2]. Titanium is mainly hosted by ilmenite sometimes coexisting with rutile. Average contents of TiO_2 in the Panimba and Mayakon samples approach those in most of

 doi:10.20944/preprints202308.0273.v1

Russia's kyanite ores: 1.00 wt % (n = 58) against 0.96 wt % [2,48]. Similarity is also observed in the average contents of CaO (0.37 wt % in the Panimba and Mayakon rocks and 0.43 wt % in metamorphics elsewhere in Russia), MnO (0.08 wt% against 0.04 wt %, respectively), and P_2O_5 (0.12 wt % against 0.02-0.30 wt %).

The complex geological history of the Transangarian segment of the Yenisey Ridge has several important implications for the feasibility of SGM production. The processes of deformation, multi-stage metamorphism of different types and grades, and magmatism produced (i) abundant andalusite schists, a rare type of alumina resources, along with kyanite and sillimanite rocks; (ii) polymineral Fe- and Al-rich metapelites in which SGM is intricately intergrown with other Al_2O_3 hosts; (iii) repeatedly altered varieties of regional metamorphic rocks (mainly andalusite-bearing); (iv) rocks with high percentages of kyanite (together with andalusite) in zones of dynamic metamorphism near thrusts; (v) thermally affected contact metamorphic rocks near the Tatar and Ayakhta plutons [50].

Much of andalusite is replaced by muscovite and margarite (Figures 7 and 9) in samples of Korda Fm. epidote-amphibolite metapelite produced by low-pressure regional metamorphism in some sites in the Panimba area. Muscovite and margarite form partial or sometimes complete pseudomorphs after fine disseminated andalusite, as well as after coarse grains of chiastolite that are potentially highly favorable for extraction. Quantitative XRD analysis of typical schists with "visible" chiastolite showed total mica percentages of ~30 % in rocks with 19.6 wt % average Al_2O_3 contents, whereas andalusite (2 to 15 wt%) is preserved in a half of such samples only. On the other hand, the phase composition of andalusite schists changes to more economically suitable in zones of contact and/or dynamic metamorphism: average mica contents decrease to 23 wt% while the percentages of Al hosts increase to 5-18 wt% andalusite, 4-29 wt% kyanite, and 20 wt% staurolite (at about same Al_2O_3 of 19.9 wt %).

5.3. Andalusite and Kyanite Concentrates

The present economic requirements to the composition of Al_2SiO_5 concentrate are very strict and increasingly restrictive, depending on uses. The unwanted components in ores and concentrate include iron oxides and sulfides (especially fine disseminated inclusions), alkalis, and titanium [3,4,6,8,51,52].

The dressing suitability of andalusite schists in Transangaria was first recognized through successful flotation experiments with samples from the Panimba ore occurrence performed in the 1960s by the Leningrad Institute of Refractories, when a concentrate composed of 36.5 wt% SiO_2, 57.1 wt% Al_2O_3, 2.2 wt% Fe_2O_3, and 1.6 wt% TiO_2 was obtained from 500 kg of rock [18]. However, the authors provided no details of the rock mineralogy, and the high-Al Teya metamorphic rocks have never been studied so far in terms of washability.

We have obtained high-grade concentrates with 86-95 % andalusite and 94-97 % kyanite from typical samples of the Teya andalusite- and andalusite-kyanite-bearing schists (Figure 19), without costly flotation and repeated separation procedures typically required in the Al_2SiO_5 production workflows. The dressing technology was based on three basic properties of ores and minerals: (i) separation of mineral intergrowths along natural grain boundaries and splitting of kyanite (and andalusite, to a lesser degree) along the cleavage; (ii) density difference between andalusite (density = 3.05 to 3.10 g/cm^3, depending on amount and type of mineral inclusions; 3.13-3.17 g/cm^3, 3.15 on average for pure andalusite), kyanite (3.56-3.67 g/cm^3, $X_{average}$ = 3.61), and other silicates (2.70-2.85 g/cm^3), except for staurolite (3.65-3.77 g/cm^3, $X_{average}$ = 3.71); (iii) magnetic susceptibility difference between Fe-bearing phases and non-magnetic Al_2SiO_5 modifications. The phase composition and features of mineral intergrowths in the Teya Al-rich schists turned out to be favorable for separation of staurolite and other Ti and Fe hosts into magnetic product (with element contents 2-7 times higher in the concentrate than in the initial rock), already at the first stage of electromagnetic separation. Crushing and milling to 0.06-0.1 mm sizes allowed extraction of Al_2SiO_5 from complex intergrowths and separation of the product from >60 μm silicate fractions (Figures 17 and 19).

Preprints (www.preprints.org) | NOT PEER-REVIEWED | Posted: 3 August 2023 doi:10.20944/preprints202308.0273.v1

The Mayakon kyanite-bearing rocks (initial contents of 13-20 % kyanite and 19-23 wt % Al_2O_3) yielded concentrates composed of 93-97 % Al_2SiO_5 (~60 wt % Al_2O_3) without flotation. Almost all mineral inclusions were removed from brittle and perfectly cleaved fine fractions of kyanite, with losses under 3 % (Figures 18 and 19).

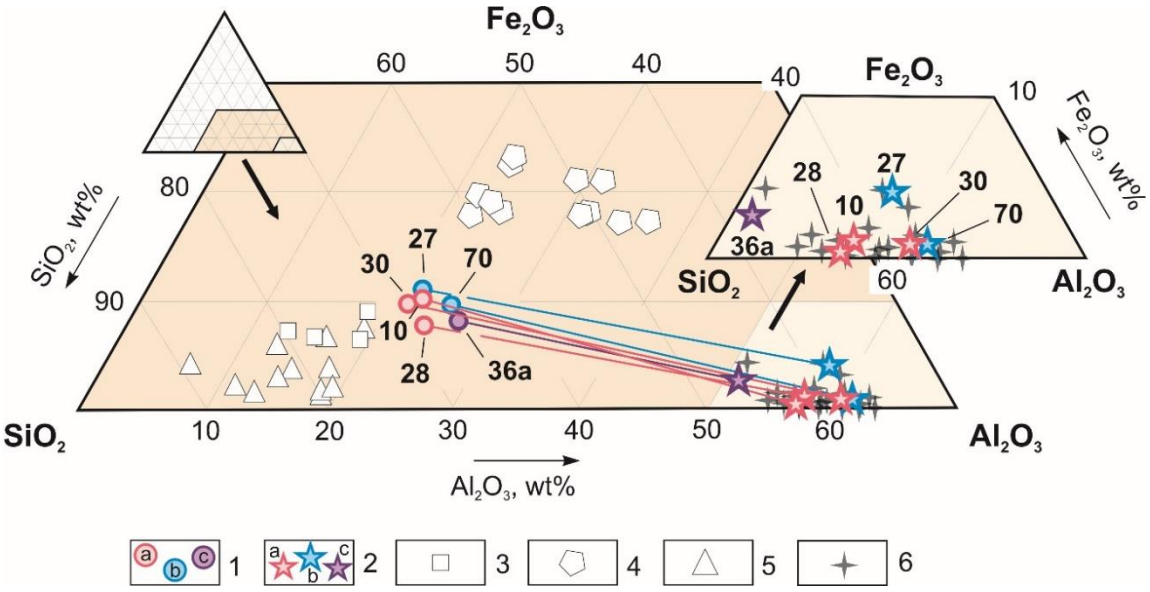

Figure 19. Compositions of bulk rocks and concentrates from Fe- and Al-metapelites of the Teya metamorphic complex in variation diagrams. 1 = initial bulk samples of andalusite-bearing (a), kyanite-bearing (b), and mixed andalusite-kyanite-bearing (c) rocks; 2-5 = beneficiation products from Panimba and Mayakon metapelite samples: 2 = final Al_2SiO_5 concentrate: andalusite (a), kyanite (b), and mixed (c); 3 = tailings; 4 – magnetic product; 5 = light product; 6 = Al_2SiO_5 concentrate from Al-rich metamorphic rocks [1; 53-57] and sand tailings with kyanite [1].

Andalusite ores have lower washability (86-92 % And; 55-59 wt % Al_2O_3), which is common to this mineral [11]. Andalusite in the sampled rocks is usually intergrown with other phases (And-Qz-Ms-Bt-St) and remained only partly separated at the applied conditions. As a result, the losses amounted to 10 % and 23 % Al_2SiO_5 in the magnetic and light products. The laboratory separation procedures we used did not allow removing all grains of quartz and silicates (Figures 13 and 15). Both andalusite and kyanite retained microinclusions (≤ 10 μm) of monazite, xenotime, zircon, ilmenite, and pyrrhotite that eluded separation into concentrate.

6. Conclusions

The revealed variability in the mineral assemblages of Panimba and Mayakon high-Al schists (at almost invariable Al_2O_3 contents of 20 wt %) means that their phase composition has to be specially monitored and taken into consideration in the evaluation of resources in different areas and strata of the Transangarian metamorphic complexes. Further exploration may be especially successful along the contact of the Korda Fm. metapelite with granitic rocks, within the so-called interior zone of metamorphism, and in zones of dynamic metamorphism adjacent to thrusts which contain quite large percentages of kyanite besides preserved andalusite.

The chemistry and mineralogy of the Al_2SiO_5 concentrate from the Teya Fe- and Al-rich metapelites fit the current viability specifications (Al_2O_3 > 56 wt %, SiO_2 < 42 wt %, Fe_2O_3 < 1 wt %, TiO_2 < 1.2 wt % and (CaO+MgO) < 0.2 wt %) and can be identified as medium-grade (up to 60 wt. %Al_2O_3). The yield of andalusite, kyanite, and mixed concentrates reached 0.7-4.1, 0.7-2.2, and 1.9-6.0 %, respectively. These values are comparable with those for andalusite ores from Scotland (0.1-2.8 %; after magnetic and gravity separation [58]), as well as kyanite ores from Karelian and Kola Peninsula in Russia (2-13 %; after flotation [2] and from Gansu province in China (7.2 %; after flotation

[53]). The grade and yield of Al_2SiO_5 concentrate from the Teya metamorphics can be improved in the future by using finer fractions of raw materials and flotation.

Author Contributions: Conceptualization, E.V.S., A.V.N., S.N.K., and I.I.L.; methodology, E.V.S., S.N.K., and A.V.N.; investigation, E.V.S., A.V.N., S.N.K., P.V.K., A.S.D., and I.I.L.; writing—original draft preparation E.V.S., S.N.K., A.V.N., and I.I.L.; visualization, A.V.N., S.N.K., and A.S.D.; supervision, I.I.L. All authors have read and agreed to the published version of the manuscript.

Funding: This research was funded by Russian Science Foundation (RSF), grant number 21-77-20018

Acknowledgments: We greatly appreciate collaboration and advice of our colleagues: Dr. P.S. Kozlov (IGG UB RAS, Ekaterinburg) for collecting representative samples and consulting; Dr. D. Kiseleva (IGG UB RAS, Ekaterinburg) for determination of trace elements in Al-rich rocks; I.Yu. Vaskova and Yu.V. Demina (Analytical Center for Multi-Element and Isotope Research, IGM, Novosibirsk, Russia) for laboratory work; M.V. Khlestov and Dr. N.S. Karmanov (IGM, Novosibirsk, Russia) for SEM analysis. Our thanks are extended to Tatiana Perepelova for helpful advice.

Conflicts of Interest: The authors declare no conflict of interest.

References

1. Lepezin, G.G. Deposits and manifestations of minerals of the sillimanite group in Russia and prospects for creating a concentrate industry based on them. *Refract. Ind. Ceram.* **1997**, *38*(7-8), 320-325.
2. Ogorodnikov, V.N., Koroteev, V.A., Voitekhovskii, Yu.L., Shiptsov, V.V., Polenov, Yu.A., Savichev, A.N., Neradovskii, Yu.N., Skamnitskaya, L.S., Bubnova, T.P., Grishin, N.N., Belogurova, O.A., Gershenkop, A.Sh., Koroteev, D.V. *Morphogenetic Types and Benefication Technology of Kyanite Ores*; Ural branch of the Russian Academy of Sciences Publ.: Ekaterinburg, Russia, 2013; pp. 1-311 (In Russ.)
3. Ihlen, P.M. Utilisation of sillimanite minerals, their geology, and potential occurrences in Norway – an overview. *Norges Geologiske Undersokelse* **2000**, *436*, 113-128.
4. Niu, F.S., Tian, L.N., Zhang, J.X., Wang, X.G. Kyanite's Status of Beneficiation Process and Application. *Adv. Mater. Res.* **2012** 602-604, 124-127.
5. Dubreuil, P., Filari, E., Sobolev, V.M. Use of andalusite refractories in ferrous metallurgy. *Refractories and industrial ceramics* **1999**, *40*(5-6), 252-259.
6. Dubreuil, P., Sobolev, V.M. Andalusite: a promising material for manufacturing high-quality refractories. *Refractories and industrial ceramics*, *40*(3-4), **1999**, 152-158.
7. Sadik, C., El Amrani, I. E., Albizane, A. Recent advances in silica-alumina refractory: A review. *J. Asian Ceram. Soc.* **2014**, *2*(2), 83-96.
8. Lepezin, G.G., Semin, V.D. Prospects for development of raw material base of the aluminum industry of Siberia. *Sov. Geol. Geophys.* **1989**, *30*(2), 77-85.
9. Lepezin, G.G., Kargopolov, S.A., Zhirakovskii, V.Y. Sillimanite group minerals: a new promising raw material for the Russian aluminum industry. *Russ. Geol. Geophys.* **2010**, *51*(12), 1247-1256.
10. Voitekhovskii Yu.L., Neradovskii Yu.N., Grishin N.N., Gershenkop A.S. Complex utilization of kyanite of the Bol'shiye Keivy as a non-traditional raw material for the alumina production. *Ekologiya Promyshlennogo Proizvodstva* **2011**, (4), 75-84. (In Russ.)
11. Overbeek, P.W. Andalusite in south africa. *J. South. Afr. Inst. Min. Metall.* **1989**, *89*(6), 157-171.
12. Lepezin, G.G., Sherman, M.L., Semin, V.D., Kravtsov, I.S. Prospects for the use of metamorphic rocks of the Altai-Sayan folded region and Yenisei range as a source of highly aluminiferous raw material. *Sov. Geol. Geophys.* **1979**, *20*(11), 26-32.
13. Likhanov, I.I. Mass-transfer and differential element mobility in metapelites during multistage metamorphism of Yenisei Ridge, Siberia. In *Metamorphic Geology: Microscale to Mountain Belts. Geological Society Special Publication*; Ferrero, S., Lanari, P., Gonsalves, P., Grosch, E. G., Eds.; Geological Society Publishing House: London, UK, **2019**, Volume 478, pp. 89-115.
14. Likhanov, I.I. Metamorphic indicators for collision, extension and shear zones geodynamic settings of the Earth's crust. *Petrol.* **2020**, 28, 1-16.
15. Likhanov, I.I. Grenville and Valhalla tectonic events at the western margin of the Siberian Craton: Evidence from rocks of the Garevka Complex, Northern Yenisei Range, Russia. *Petrol.* **2022,** *30*, S72-S100.
16. Likhanov, I.I., Santosh, M. The "triple point" paradigm of aluminosilicates revisited. *Geol. J.* **2020**, *55*, 4772-4789.
17. Likhanov, I.I., Polyansky, O.P., Reverdatto, V.V., Memmi, I. Evidence from Fe- and Al-rich metapelites for thrust loading in the Transangarian Region of the Yenisey Ridge, eastern Siberia. *J. Metamorph. Geol.* **2004**, *22*, 743-762.

18. Kozlov, P.S., Lepezin, G.G. Petrology, petrochemistry, and metamorphism of the rocks in the Angara region of the Yenisei Ridge. *Russ. Geol. Geophys.* **1995**, *36*(5), 1-21.
19. Kozlov, P.S. High-alumina nonbauxite rocks of the Trans-Angara Segment of the Yenisei Ridge: composition, trends and application potential. *News Ural State Min. Univ.* **2018**, *1*(49), 39-45.
20. Kozlov, P.S. Geology and tectono-metamorphic evolution of the Precambrian complexes of the western margin of the Siberian Craton (North Yenisei Ridge). PhD thesis, The Zavaritsky Institute of Geology and Geochemistry, Yekaterinburg, 2021. (In Russ.)
21. Likhanov, I.I., Kozlov, P.S., Popov, N.V. Ferruginious-aluminous metapelites of the North Yenisei Ridge: Formation paleosettings, nature and age of protolith. *Lithosphere (Russia)* **2022**, 22(4), 448-471. (In Russ.)
22. Kozlov, P.S., Likhanov, I.I., Reverdatto, V.V., Sukhorukov V.P. Petrogenesis, georesourses, and prospects for practical use of high-aluminous rocks of the North Yenisei Ridge (East Siberia). *Geosphere Res.* **2022**, 4, 6-35. (In Russ.)
23. Brovkov, G.N., Li, L.V., Sherman, M.L. *Geology and Metallogeny of the Yenisei Ore Belt*; Siberian Research Institute of Geology, Geophysics and Mineral Raw Materials Publ.: Krasnoyarsk, Russia, 1985; pp. 1-291. (In Russ.)
24. Nikulov, L.P., Babkin, A.N., Kolyamkin, V.M., Leshchinsky, S.L., Serzhantov, N.F., Rakhmatullin, R.N. *State Geological Map of Russia, Scale 1:200,000, Ser. Yenisei, Sheet O-46-XXVIII (Bol. Murta). Explanatory Note*; Krasnoyarskgeols'yemka: Moscow, Russia, 2002.
25. Likhanov, I.I., Reverdatto, V.V. Mass transfer during andalusite replacement by kyanite in Al- and Fe-rich metapelites in the Yenisei Range. *Petrol.* **2002**, *10*, 479-494.
26. Likhanov, I.I., Reverdatto, V.V., Kozlov, P.S., Khiller, V.V., Sukhorukov, V.P. P-T-t constraints on polymetamorphic complexes of the Yenisey Ridge, East Siberia: implications for Neoproterozoic paleocontinental reconstructions. *J. Asian Earth Sci.* **2015**, *113*, 391-410.
27. Likhanov, I.I., Nozhkin, A.D., Reverdatto, V.V., Krylov, A.A., Kozlov, P.S., Khiller, V.V. Metamorphic evolution of ultrahigh-temperature Fe- and Al-rich granulites in the South Yenisey Ridge and tectonic implications. *Petrol.* **2016**, *24*, 392-408.
28. Likhanov, I.I., Santosh, M. Neoproterozoic intraplate magmatism along the western margin of the Siberian Craton: implications for breakup of the Rodinia supercontinent. *Precambrian Res.* **2017**, *300*, 315-331.
29. Xiao, W., Kusky, T., Safonova, I., Seltmann, R., Sun, M. Tectonics of the Central Asian Orogenic Belt and its Pacific analogues. *J. Asian Earth Sci.* **2015**, *113*, 1-6.
30. Vernikovsky, V.A., Vernikovskaya, A.E., Kotov, A.B., Sal'nikova, E.B., Kovach, V.P. Neoproterozoic accretionary and collisional events on the western margin of the Siberian craton: new geological and geochronological evidence from the Yenisey Ridge. *Tectonophys.* **2003**, 375, 147-168.
31. Likhanov, I.I., Reverdatto, V.V., Kozlov, P.S., Vershinin, A.E. The Teya polymetamorphic complex in the Transangarian Yenisei Ridge: an example of metamorphic superimposed zoning of low- and medium-pressure facies series. *Dokl. Earth Sci.* **2011**, *436*, 213-218.
32. Likhanov, I.I., Régnier, J.-L., Santosh, M. Blueschist facies fault tectonites from the western margin of the Siberian Craton: Implications for subduction and exhumation associated with early stages of the Paleo-Asian Ocean. *Lithos* **2018,** *304-307*, 468-488.
33. Likhanov, I.I., Nozhkin, A.D., Savko, K.A. Accretionary tectonics of rock complexes in the eastern margin of the Siberian Craton. *Geotecton.* **2018**, *52*, 22-44.
34. Likhanov, I.I., Santosh, M. A-type granites in the western margin of the Siberian Craton: implications for breakup of the Precambrian supercontinents Columbia/Nuna and Rodinia. *Precambrian Res.* **2019,** *328*, 128-145.
35. Likhanov, I.I., Nozhkin, A.D., Reverdatto, V.V., Kozlov, P.S. Grenville tectonic events and evolution of the Yenisey Ridge at the western margin of the Siberian Craton. *Geotecton.* **2014**, *48*, 371-389.
36. Likhanov, I. I. Mineral Reactions in Aluminous and Ferruginous Hornfels in Relation with the Problem of Stability of Rare Contact Metamorphism Mineral Assemblages. *Russ. Geol. Geophys.* **2003**, *44*, 305-316.
37. Nekrasova, N.A. Geology and genesis of the Panimba deposit (Yenisei Ridge). PhD thesis, Siberian Federal University, Krasnoyarsk, 2019. (In Russ.)
38. Kozlov, P.S. Problems of petrology and petrochemistry of andalusite schists of the Trans-Angara segment of the Yenisei Ridge (on the example of the Panimbinsk deposit). In *Problems of Geology and Metallogeny of the Krasnoyarsk Krai*. Nauka: Novosibirsk, Russia, 1989; pp. 89-100. (In Russ.).
39. Kozlov, P.S. Petrology and petrochemistry of metapelites of the Transangaria of the Yenisei Ridge: PhD thesis, United Institute of Geology, Geophysics and Mineralogy, Novosibirsk, Russia, 1994. (In Russ.)
40. Hietanen, A. On the facies series in various types of metamorphism. *J. Geol.* **1967**, *75*, 187-214.
41. Likhanov, I.I., Reverdatto, V.V., Selyatitskii, A.Y. Mineral equilibria and P–T diagram for Fe–Al metapelites in the KFMASH system (K_2O–FeO–MgO–Al_2O_3–SiO_2–H_2O). *Petrol.* **2005**, *13*(1), 73-83.

42. Shatsky, V., Sitnikova, E., Kozmenko, O., Palessky, S., Nikolaeva, I., Zayachkovsky, A. Behavior of incompatible elements during ultrahigh-pressure metamorphism (by the example of rocks of the Kokchetav massif). *Russ. Geol. Geophys*. **2006**, *47*, 482–496. Kiseleva, D., Shilovsky, O., Shagalov, E., Ryanskaya, A., Chervyakovskaya, M., Pankrushina, E., Cherednichenko, N. Composition and structural features of two Permian pararеptile (Deltavjatia vjatkensis, Kotelnich Site, Russia) bone fragments and their alteration during fossilisation. *Palaeogeogr. Palaeoclimatol. Palaeoecol.* **2019**, *526*, 28-42.
43. Warr, L.N. IMA–CNMNC approved mineral symbols. *Mineral. Mag*. **2021**, *85*(3), 291-320.
44. Rudnick R.L., Gao S. Composition of the Continental Crust. *Treat. Geochem*. **2003**, *3*, 1-64.
45. Ogorodnikov, V.N., Polenov, Yu.A., Savichev, A.N. Rare metals and rare earth elements in kyanite ore from Kola Peninsula and Ural. *Trudy Instituta geologii i geokhimii im. akad. A.N. Zavaritskogo* **2013**, *160*, 274-281. (In Russ.)
46. Espenshade, G.A., Potter, D.B. Kyanite, sillimanite and andalusite deposits of the Southeastern States. *United States Geol. Surv. Prof. Pap.* **1960**, *336*, 1-21.
47. Koroteev, V.A., Ogorodnikov, V.N., Voitekhovskii, Yu.L., Polenov, Yu.A., Savichev, A.N., Shiptsov, V.V., Sazonov, V.N., Koroteev, D.V. *Non-Bauxite Aluminum Raw Materials of Russia*; Ural branch of the Russian Academy of Sciences Publ.: Ekaterinburg, Russia, 2011; 227 p. (In Russ.)
48. Stepanov, S.A. Metamorphism, Formation Conditions, and Prospects for High-Alumina Raw Materials of the Bazybai. PhD thesis, United Institute of Geology, Geophysics and Mineralogy, Novosibirsk, 2005. (In Russ.)
49. Likhanov, I.I., Reverdatto, V.V., Sheplev, V.S., Verschinin, A.E., Kozlov, P.S. Contact metamorphism of Fe- and Al-rich graphitic metapelites in the Transangarian region of the Yenisei Ridge, eastern Siberia, Russia**.** *Lithos* **2001,** *58*(1-2), 55-80**.**
50. *The Economics of Kyanite*. London: Roskill Information Services Ltd, UK, 1990; pp. 118.
51. Indian Minerals Yearbook – 2019. New Delhi: Government of India. Indian Minerals Yearbook ministry of Mines.
52. Zhao, J., Jia J., Wang, W., Cao, G., Zhang, F., Li, J. Experimental Study on Mineral Processing of Kyanite Ore in Saerhabutale in Gansu Province. *Multipurp. Utiliz. Miner. Res.* **2017**, (6), 72-77.
53. Bulut, G., Yurtsever, C. Flotation behaviour of Bitlis kyanite ore. *Int. J. Miner. Process.* **2004**, *73*(1), 29-36.
54. Zhou, L., Zhang, Y. Andalusite flotation using alkyl benzene sulfonate as the collector. *Miner. Process. Extr. Metall. Rev.*, **2011**, *32*(4), 267-277.
55. Zhou, L.C., Zhang, Y.M. Flotation separation of Xixia andalusite ore. *Trans. Nonferr. Metal. Soc. China* **2011**, *21*(6), 1388-1394.
56. Gogou, A., Mavrogonatos, C., Anastasatou, M., Voudouris, P., Chryssoulis, S., Stamatakis, M. Beneficiation Process of Kyanite-Rich Mineral Assemblages from Thassos Island Aegean Sea, Greece. *Miner. Process. Extr. Metall. Rev.* **2021**, *43*(7), 899-909.
57. Mitchell, C.J., Harrison, D.J. *Industrial Mineral Potential of Andalusite and Garnet in the Scottish Highlands*. Nottingham: British Geological Survey Publ., UK, 1997; pp. 1-70.